Fast and Selective β-C–H Borylation of N-Heterocycles with a Supramolecular Iridium Catalyst: Circumventing Deactivation Pathways and Mechanistic Insights

Jonathan Trouvé, Purushothaman Rajeshwaran, Michele Tomasini, Antoine Perennes, Thierry Roisnel, Albert Poater, Rafael Gramage-Doria

Fast and Selective β-C-H Borylation of N-Heterocycles with a Supramolecular Iridium Catalyst: Circumventing Deactivation Pathways and Mechanistic Insights

Jonathan Trouvé,[a] Purushothaman Rajeshwaran,[a] Michele Tomasini,[b] Antoine Perennes,[a] Thierry Roisnel,[a] Albert Poater,*[b] and Rafael Gramage-Doria*[a]

[a]Univ Rennes, CNRS, ISCR – UMR 6226, F-35000 Rennes, France

[b]Institut de Química Computacional i Catàlisi, Departament de Química, Universitat de Girona, c/Mª Aurèlia Capmany 69, 17003 Girona, Catalonia, Spain

KEYWORDS. supramolecular catalysis, C-H borylation, iridium, nitrogen, porphyrins

ABSTRACT: Selective iridium-catalyzed C-H bond borylations of unbiased or directing-group-free substrates typically occur under long reaction times and mild temperatures in order to avoid unselective processes including catalyst deactivation. Herein, we describe a supramolecular approach that enables the C-H bond borylation of challenging pyiridines and imidazoles in very short reaction times (up to 2 hours) with a negligible incubation period for catalyst activation. The catalyst is based on a highly rigid zinc-porphyrin substrate-recognition site in the secondary coordination sphere and a triazolopyridine chelating fragment attached to the first coordination sphere at iridium. The borylation occurs at the C-H bond from the substrate located at four chemical bonds apart from the molecular recognition site with the selectivity being exclusively imposed by the distance between the active site and the molecular recognition site regardless of the nature of the *N*,*N*-chelating fragment coordinating to iridium as further supported by DFT calculations. Additional studies (control experiments, NMR, SCXRD) unraveled key catalyst deactivation pathways in which up to three different partners (water, methoxide ligands from the iridium precursor and the triazolopyridine fragment) compete with the *N*-heterocycle substrate for binding to the molecular recognition site of the supramolecular catalyst. This fundamental understanding made possible the identification of a supramolecular catalyst featuring a 4-methyl substitution pattern in the first coordination sphere at iridium that provides a suitable balance of steric and electronic effects in both primary and secondary coordination spheres, thereby bypassing the manifold catalyst deactivation pathways. DFT calculations further indicated the importance of non-covalent interactions beyond the molecular recognition site on the stabilization of the different intermediates and transition sates.

INTRODUCTION

The efficient production of chemicals at will in a sustainable manner is of high interest for industrial and academic laboratories.[1] As such, the last century has witnessed tremendous efforts devoted to the development of catalytic technologies for such purposes.[2] In this context, homogeneous transition metal-catalyzed processes occupy a central place since the ease of ligand fine-tuning is advantageous to disclose new reactivity patterns.[3] Most of these transformations require the use of pre-activated coupling partners to selectively form new carbon-carbon or carbon-heteroatom bonds at specific positions at the expenses of generating substantial amounts of side-products including those from the pre-activation reactions too.[4] In this regard, transition metal-catalyzed C-H bond functionalizations have revolutionized in the last decades the way to conceive chemical synthesis by providing unprecedented bond disconnections and novel bond-forming processes.[5] Currently, a myriad of methodologies exist for C-H bond functionalizations by means of transition metal catalysts.[6] However, most of them rely on the intrinsic reactivity of substrates to reach a precise C-H bond activation or by exploiting directing groups introduced in previous steps to the molecule of interest to bring the metal catalyst at close proximity of the C-H bond to be functionalized.[7] It is clear from a sustainable point of view, that the avoidance of directing groups for C-H bond functionalizations in unbiased substrates needs to be urgently addressed.[8]

From the many transition metal-catalyzed C-H functionalization strategies, metal-catalyzed C-H borylations are extremely appealing.[9] Indeed, the newly created C-B bond is a readily transformable moiety towards the formation of carbon-carbon and carbon-heteroatom bonds by using well-established methodologies.[10] Besides the use of rhodium,[11] platinum,[12] cobalt,[13] nickel[14] or lanthanide catalysts,[15] the iridium catalysts are exceptionally active enough to tackle the functionalization of C-H bonds belonging to highly inert aliphatic and aromatic fragments without the requirements to introduce directing groups in the substrates.[16] Consequently, the site-, regio- and enantio-selectivity of such reactions have been a challenging focus of research because the bond dissociation energies associated for discriminating those C-H bonds lie on a narrow range.[17] As pioneered by Hartwig and Ishiyama, the iridium-coordinated *N*,*N*-bipyridine frameworks appear to be the most powerful family of ligands for iridium-catalyzed C-H borylation reactions.[18] For instance, 4,4'-di-*tert*-butyl-2,2'-bipyridine (**dtbpy**, **Figure 1A**) and phenantroline-type ligands

are considered the most suitable ligand for enabling the iridium-catalyzed borylation of aromatic as well as heteroaromatic C-H bonds using bis(pinacolato)diboron (B_2pin_2) as the borylating agent.[19] Recently, modified versions from the dtbpy ligand have been disclosed in order to reach unprecedented, remote regio- and site-selectivities by introducing in the secondary coordination sphere of the catalyst a variety of functional groups that enable molecular recognition with functional groups from the aromatic substrate *via* hydrogen bonding or ion pairing.[20]

In the case of nitrogen-containing heterocyclic substrates, the challenge is upgraded substantially since the nitrogen lone pair from these compounds can over coordinate to the iridium catalyst, thus preventing productive borylation to occur.[21] Although powerful and selective C-H bond borylation of azines, typically pyridines, have been reported by the groups of Hartwig and Ishiyama,[22] Nakao,[23] Maleczka and Smith,[24] Marder and Steel,[25] ourselves,[26] and others,[27] extensive long reaction times are required (i.e. 16 to 72 hours, **Figure 1B-1C**). This is due to (1) the significant incubation period that the pre-catalyst needs in order to form the active iridium tris-boryl catalytic species[28] and (2) the mild reaction conditions (i.e. low temperature, **Figure 1B**) that are required to avoid unselective transformations that would result in a mixture of borylated compounds or other side-products resulting from product decomposition.[29] Overall, increasing catalyst performance by reducing reaction time while keeping high levels of selectivity remains a major breakthrough to be addressed in iridium-catalyzed C-H borylation of unbiased substrates. In the following, we present a supramolecular iridium catalyst that circumvents these above-stated limitations resulting in a highly productive and selective system for the C-H bond borylation of pyridines in unprecedented, short reaction times up to 2 hours while operating at high a temperature of 100 °C (**Figure 1D**). The catalyst features a zinc-porphyrin molecular recognition site in the secondary coordination sphere and it was selected after thorough experimentation to identify, and further avoidance of, catalyst deactivation pathways. In particular, we demonstrate that the pyridine substrates compete with (i) water, (ii) the methoxide ligand from the iridium precursor and (iii) the triazolopyridine fragment from the first coordination sphere of the catalyst, for binding to the molecular recognition pocket. By ligand fine-tuning and precise control of reaction conditions, we found that a 4-methyl-substituted pattern in the first coordination sphere of the catalyst outperforms existing state-of-the-art iridium catalysts for the *β*-selective C-H bond borylation of nitrogen-containing heterocycles (**Figure 1D**). Importantly, the supramolecular design of the catalyst enables the C-H bond borylation at a precise distance of four chemical bonds apart from the molecular recognition site regardless of the nature of the *N*,*N*-chelating unit coordinating to iridium as further supported by computational studies, thereby demonstrating the power of secondary coordination spheres to control both activity and selectivity for challenging transformations. The subtlety of the supramolecular catalysis was highlighted by the presence of additional set of non-covalent interactions involving the porphyrin backbone beyond the molecular recognition site according to in-depth DFT calculations performed for understanding the key intermediates and transition states.

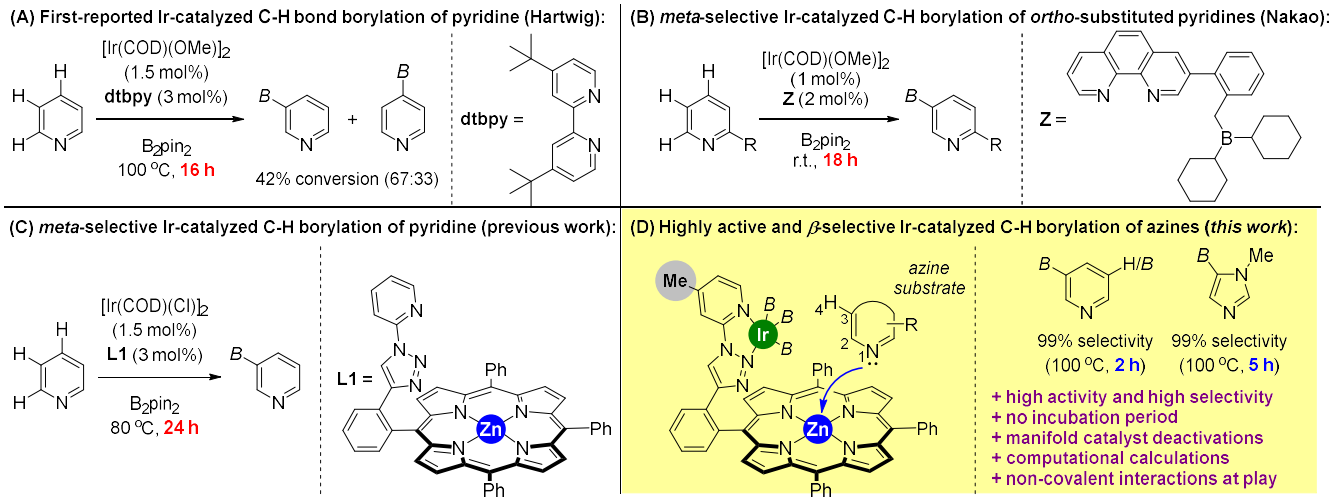

Figure 1. First-reported iridium-catalyzed C-H borylation of pyridine (**A**), previous strategies to reach *meta*-selective C-H borylation of pyridines under long reaction times (**B** and **C**), and the supramolecular iridium-catalyzed C-H borylation developed in this study (**D**). *B* = (pinacolato)boron.

RESULTS AND DISCUSSION

Synthesis, characterization and supramolecular coordination chemistry studies of supramolecular ligands L1-L6. Since the C-H bond activation event appears to be the rate-determining step for this type of catalysis according to computational calculations,[30] we anticipated that the fine-tuning at the first-coordination sphere around the iridium center would be beneficial in terms of reactivity. As such, we synthesized the supramolecular ligands **L1**-**L6** according to our preliminary findings,[26] in which a key alkylnyl-substituted zinc-porphyrin **1** is engaged in a copper-catalyzed click reaction with a 2-azido-substituted pyridine derivative (**Scheme 1**). In this manner, the supramolecular catalysts **L1**-**L6** featuring different electronic and steric patterns (H, 4-^{t}Bu, 4-Me, 6-Me, 4-OMe, 4-CF_3) in the pyridine ring that will be involved in the coordination to iridium were obtained and characterized by NMR spectroscopy as well as HRMS studies.[31]

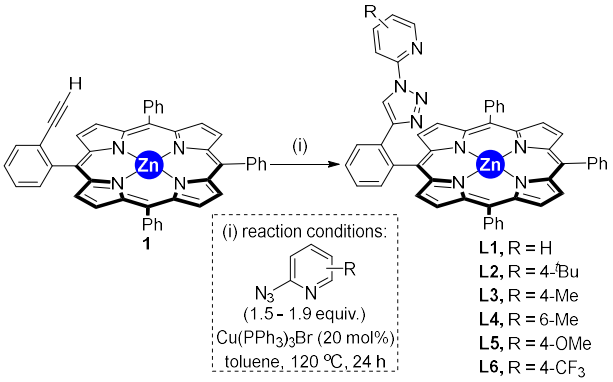

Scheme 1. Synthesis of the supramolecular ligands **L1**-**L6**.

Next, we evaluated the ability of these ligands to interact with pyridine derivatives *via* kinetically labile Zn···N interactions.[32] ^{1}H NMR spectroscopy studies were performed combining equimolar amounts of unfunctionalized pyridine (**1a**) with each ligand **L1**-**L6**, respectively, in a $CDCl_3$ solution at room temperature (**Table 1**).[31] A representative case is shown in **Figure 2** for the self-assembly of the bulkiest ligand (**L4**) with pyridine ([**L4** ⊂ **1a**]). In all cases, the three pyridine proton signals underwent remarkable up-field shifts as shown in **Table 1**, indicating an interaction to the zinc-porphyrin core *via* apical Zn···N coordination (Supporting Information, Figures S1-S6).[33] The formation of a single species in solution points out that the binding of the pyridine is fast at the NMR timescale and it is in exchange between a coordination at the same face where the triazolopyridine ring lies and a coordination at the opposite face (top-bottom equilibria, **Scheme 2**). According to previous observations by us and others,[26,32] the binding constant between these supramolecular ligands and pyridine is estimated in the range of $K_{1:1}$ *ca.* 10^3-10^4 M^{-1}. In addition DOSY studies carried out with all supramolecular ligands **L1**-**L6**, respectively, in the presence of equimolar amounts of pyridine also evidenced the dynamic binding of the pyridine substrate to the supramolecular ligand (Supporting Information, Figures S7-S18).[31]

Table 1. Chemical shifts (δ in ppm) corresponding to pyridine (**1a**) upon equimolar binding to the supramolecular ligands **L1**-**L6**.[a]

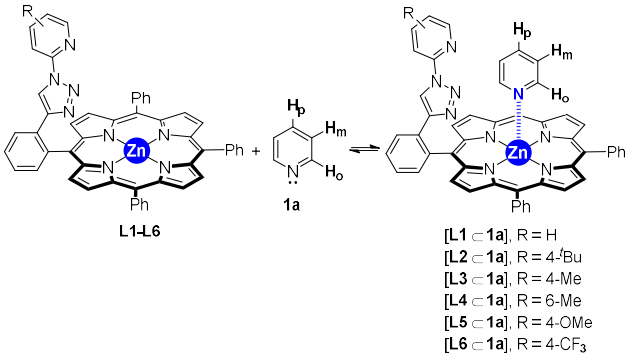

Compound	**H$_o$** (δ, ppm)	**H$_m$** (δ, ppm)	**H$_p$** (δ, ppm)
pyridine **(1a)**	8.56	7.60	7.22
[L1 ⊂ 1a]	4.15	5.86	6.51
[L2 ⊂ 1a]	4.30	5.93	6.58
[L3 ⊂ 1a]	4.80	6.08	6.71
[L4 ⊂ 1a]	4.60	6.00	6.63
[L5 ⊂ 1a]	4.79	6.10	6.75
[L6 ⊂ 1a]	4.82	6.11	6.74

[a] ^{1}H NMR spectroscopy experiments performed in $CDCl_3$ (400 MHz, 298 K).

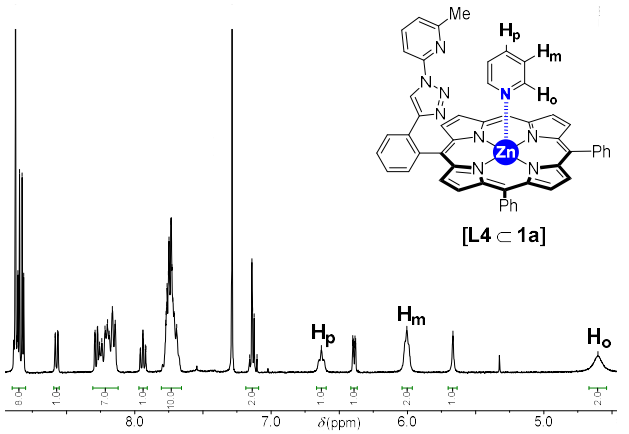

Figure 2. ^{1}H NMR spectrum ($CDCl_3$, 400 MHz) of the self-assembly **[L4 ⊂ 1a]** in an equimolar ratio.

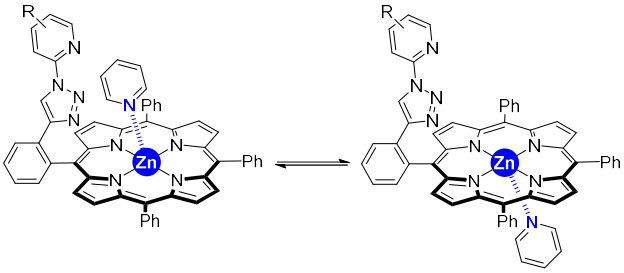

Scheme 2. Top-bottom side equilibria for the binding of pyridine to the supramolecular ligands.

The molecular structure of **L1** was further confirmed by X-ray diffraction studies performed in single crystals obtained from a concentrated solution in undistilled 1,2-dichloroethane. The compound **L1** crystallizes with one water molecule binding to the zinc atom (**Figure 3**) which is further involved in an intramolecular hydrogen bonding with the nitrogen atom (N1) from the pyridine ring ($d_{O\text{-}H\cdots N1}$ = 2.006 Å). In the solid state the system forms a supramolecular polymer stabilized by additional intermolecular hydrogen bonding with the nitrogen atom (N4) from the triazole motif ($d_{O\text{-}H\cdots N4}$ = 2.155 Å, see Figures S43 and S44 in the Supporting Information).[31] As such, it is clear that traces of water need to be avoided to further enhance the binding of pyridine to the zinc-porphyrin site, especially during the catalytic experiments that operate at high temperature (*vide infra*), thereby identifying the water binding to the molecular recognition site as an undesired deactivation pathway.[34]

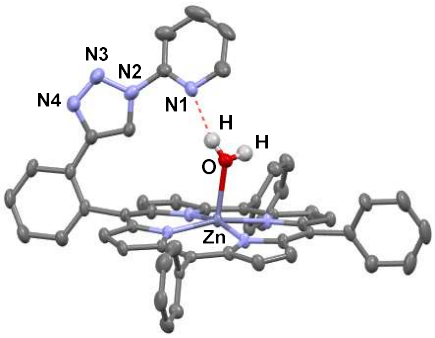

Figure 3. ORTEP of assembly [**L1** ⊂ **H$_2$O**] determined by single-crystal X-ray diffraction studies with thermal ellipsoids at 50% probability indicating hydrogen bonding in dashed lines (red). All hydrogen atoms except of those of water as well as 1,2-dichloroethane solvent molecules are omitted for clarity.

Assessment of the iridium precursor for the supramolecular *meta*-selective C-H borylation of pyridine. A vast number of studies regarding iridium-catalyzed C-H borylation of unbiased and directing-group-free substrates have demonstrated the superior reactivity encountered when using [Ir(COD)(OMe)]$_2$ (COD = 1,5-cyclooctadiene) over [Ir(COD)(Cl)]$_2$ as the precursor for generating the active cationic iridium(I) species with *N*,*N*-chelating ligands derived from the 2,2'-bipyridine family.[18-25,27,28] The main reasons were ascribed to (1) the increased lability of the Ir-OMe bond with respect to the more thermodynamically stable Ir-Cl bond and (2) the formation of catalytically active iridium tris-boryl species in the presence of B$_2$pin$_2$ by release of MeO-Bpin side-product which is energetically more favorable than the corresponding Cl-Bpin countepart.[35] Alternatively, Colacot and co-workers demonstrated that [Ir(COD)(Cl)]$_2$ might be a suitable precursor in THF solvent as it generates a catalytically active iridium species that compare well with those derived from using [Ir(COD)(OMe)]$_2$.[36] In our case, the supramolecular catalysis was only effective in the presence of aromatic, non-polar solvents (i.e. *p*-xylene or toluene) that solubilize well the supramolecular ligand and that do not perturb the weak Zn···N-pyridine interaction.[26] Surprisingly, we noted that [Ir(COD)(Cl)]$_2$ precursor was more appropriate than [Ir(COD)(OMe)]$_2$ with our supramolecular ligands (**Table 2**). For instance, using the supramolecular ligand **L1** at 80 °C, the C-H borylation of pyridine (**1a**) was finished in 12 hours with a remarkable reactivity that leads mainly to the bis-borylated product **2aa** with the [Ir(COD)(Cl)]$_2$ precursor (**Table 2**, entry 1), whereas the reaction with [Ir(COD)(OMe)]$_2$ precursor did not reach completion even after 24 hours affording a modest 73% conversion with major formation of the mono-borylated product **2a** (**Table 2**, entry 2), the remaining 27% corresponds to unreacted pyridine **1a** starting material. In both cases, the regio-selectivity was directed towards the *meta*-borylated products **2a** and **2aa** with undetectable formation of *para*- or *ortho*-isomers **3a** and **4a**, respectively (**Table 2**, entries 1-2). Note that no C-H borylation occurs if the triazolopyridine fragment is not covalently-linked to the zinc-porphyrin scaffold.[26]

Table 2. Influence of the iridium precursor in the supramolecular *meta*-selective C-H borylation of pyridine.[a]

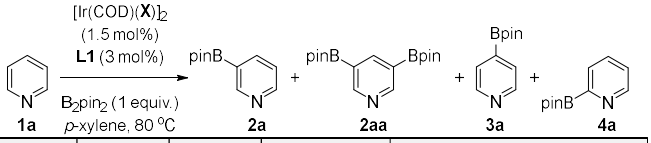

Entry	X	Time	Conv.[b]	2a : 2aa : 3a : 4a (%)[c]
1	Cl	12 h	>99 %	40 : 60 : 0 : 0
2	OMe	24 h	73 %	75 : 25 : 0: 0

[a] Reaction conditions: pyridine (0.162 mmol), B$_2$pin$_2$ (0.162 mmol), [Ir(COD)(Cl)]$_2$ (1.5 mol%), **L1** (3 mol%), *p*-xylene (1 mL), 80 °C. [b] Conversion determined as pyridine consumption, the remaining % corresponds to unreacted pyridine starting material. [c] Ratio of borylated products determined by ^{1}HNMR and GC using *n*-dodecane as internal standard.

In order to further understand such unexpected, reversed behavior when compared to literature precedents,[18-25,27,28,35,36] we designed a series of experiments to verify whether the anionic methoxide ligand from the iridium precursor [Ir(COD)(OMe)]$_2$ could bind to the zinc-porphyrin molecular recognition site *via* Zn···O-Me interaction considering the known oxophilicity displayed by zinc-porphyrin derivatives,[37] thereby competing eventually with the pyridine substrate for the same binding site. The supramolecular ligand **L1** was treated with 0.5 equivalents of [Ir(COD)(OMe)]$_2$ at room temperature in a toluene-d_8 solution (similar solvent as used for the catalytic experiments) and the resulting ^{1}H NMR spectrum displayed a methoxide signal at δ = 2.14 ppm, which is up-field shifted when compared to the methoxide signal from the starting iridium precursor that resonates at δ = 3.12 ppm (Supporting Information, Figures S19-S24).[31] In addition, whereas the carbon signal belonging to the methoxide ligand in the [Ir(COD)(OMe)]$_2$ precursor appears as a well-resolved singlet

at δ = 56 ppm in its $^{13}C\{^1H\}$ NMR spectrum, in the case of combining $[Ir(COD)(OMe)]_2$ precursor with **L1**, the signal belonging to the methoxide ligand was not detectable likely due to broadening (Supporting Information, Figure S25).[31] Such methoxide effect was not observed when performing NMR experimentation with **dtbpy** and 0.5 equivalents of $[Ir(COD)(OMe)]_2$ (Supporting Information, Figure S26).[31] For comparison purposes, **L1** was mixed with 1 equivalent of potassium *tert*-butoxide (sodium methoxide and potassium methoxide were poorly soluble in toluene solution) and its ^1H and $^{13}C\{^1H\}$ NMR spectra displayed similar trends as observed for the methoxide ligand: the singlet belonging to *tert*-butyl group was slightly upfield shifted in the presence of **L1** ($\Delta\delta$ = 0.03 ppm in the ^1H NMR spectrum and $\Delta\delta$ *ca.* 6 ppm in the $^{13}C\{^1H\}$ NMR spectrum – a downfield of $\Delta\delta$ *ca.* 1 ppm was observed for the *C*-O signal in the $^{13}C\{^1H\}$ NMR spectrum, see Supporting Information, Figures S27-S35).[31] These observations indicate that the methoxide ligand is oxophilic enough for binding in a reversible manner to the zinc-porphyrin site from the supramolecular ligand **L1** *via* Zn···O-Me interaction (**Scheme 3**), thereby establishing the suitability of the, typically less employed, $[Ir(COD)(Cl)]_2$ as the ideal precursor for this particular supramolecular catalysis.[38]

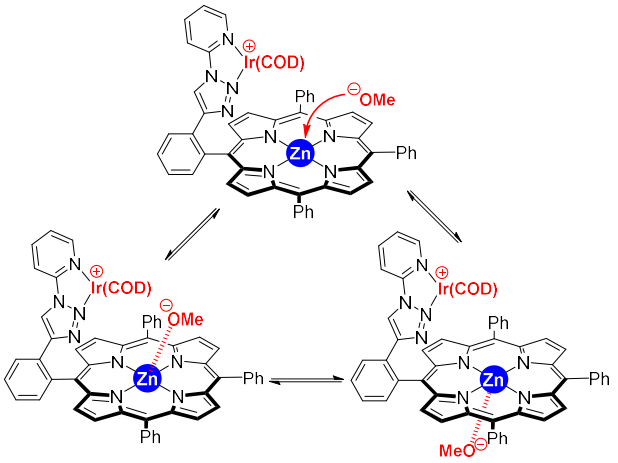

Scheme 3. Catalyst deactivation pathway *via* methoxide binding to the zinc-porphyrin site from supramolecular ligand **L1** in the presence of 0.5 equivalents of $[Ir(COD)(OMe)]_2$ precursor according to NMR spectroscopy studies (the zinc oxidation state is formally +2).

Evidence for the involvement of the triazolopyridine fragment in a deactivation pathway. As above-discussed in the introductory section of this contribution, **dtbpy** derivatives including phenantroline-type ones are prominently used as superior ligands for iridium-catalyzed borylations.[18-25,27,28] Consequently, the parent supramolecular version, namely **L2** (**Scheme 1**), which contains a *tert*-butyl group in *para* position of the triazolopyridine ring, was employed as a prospective ligand in the iridium-catalyzed C-H bond borylation of pyridine **1a** (**Table 3**). Unexpectedly, the catalysis was inefficient with a conversion of **1a** not exceeding 5% at 80 °C when employing **L2** (**Table 3**, entry 2), whereas the supramolecular ligand **L1** afforded full conversion (**Table 3**, entry 1). Even at high temperatures of 100 °C and 120 °C (**Table 3**, entries 3-4), the conversions of **1a** by using **L2** did not surpass 15% with a same *meta*-selectivity as observed for **L1**. In the same vein, the catalysis was completely unsuccessful at lower temperatures with **L1** and **L2**, respectively (**Table 3**, entries 5-6).

Table 3. Initial ligand assessment of the supramolecular iridium-catalyzed *meta*-selective C-H borylation of pyridine.[a]

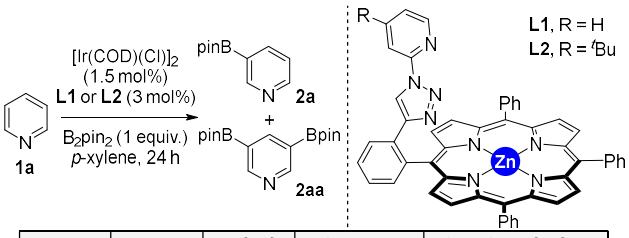

Entry	L	T (°C)	Conv.[b]	2a : 2aa (%)[c]
1	**L1**	80	>99 %	40 : 60
2	**L2**	80	5 %	100 : 0
3	**L2**	100	10 %	100 : 0
4	**L2**	120	15 %	100 : 0
5	**L1**	20	0 %	-
6	**L2**	20	0 %	-

[a] Reaction conditions: pyridine (0.162 mmol), B_2pin_2 (0.162 mmol), $[Ir(COD)(Cl)]_2$ (1.5 mol%), **L** (3 mol%), *p*-xylene (1 mL), 24 h. [b] Conversion determined as pyridine consumption, the remaining % corresponds to unreacted pyridine starting material. [c] Ratio of borylated products determined by ^{1}HNMR and GC using *n*-dodecane as internal standard.

Considering such contra-intuitive reactivity of **L1** and **L2**, together with the relatively short distance existing between the triazolopyridine fragment and the zinc-porphyrin site in the X-ray structure of [**L1**⊂H_2O] (*vide supra*) as well as a chemical shift dependency observed by ^{1}HNMR at different concentrations of **L1**,[26] we decided to investigate the potential coordination of the triazolopyridine fragment to the zinc-porphyrin site as a catalyst deactivation pathway in this supramolecular catalysis. Such plausible event might be enhanced by the presence of a strong electro-donating substituent as it is the case for **L2**, which presents a *tert*-butyl group in *para* position of the iridium-coordinating pyridine ring. To this aim, ^{1}H NMR spectroscopy studies were performed in $CDCl_3$ at room temperature by combining equimolar amounts of zinc-tetraphenylporphyrin (**ZnTPP**) with triazolopyridine **L1*** and **L2*** (**Scheme 4**), respectively, which are the corresponding molecular components of the supramolecular ligands **L1** and **L2**.[31] In both cases, albeit small, significant up-field shifts were observed (0.04 ppm > $\Delta\delta$ > 0.01 ppm) for the signals belonging to the triazole C-H proton (H_{tr}) and the *ortho*-pyridinic proton (H_{op}) from **L1*** and **L2***, respectively, upon interaction with **ZnTPP** (Supporting Information, Figures S36-S42).[31] It is worthy to mention at this stage that five-membered ring azines are well-known to bind to zinc-porphyrins[26,39] whilst *ortho*-substituted pyridine derivatives exhibit negligible binding to zinc-porphyrins.[26,32,40] As such, it is reasonable to assume that the triazole unit is engaged in a kinetically labile Zn···N interaction with **ZnTPP** (**Scheme 4**). In principle, both nitrogen atoms N3 and N4, (see atom numbering in **Figure 3** too) can be involved in the reversible coordination to zinc (**Scheme 4**).

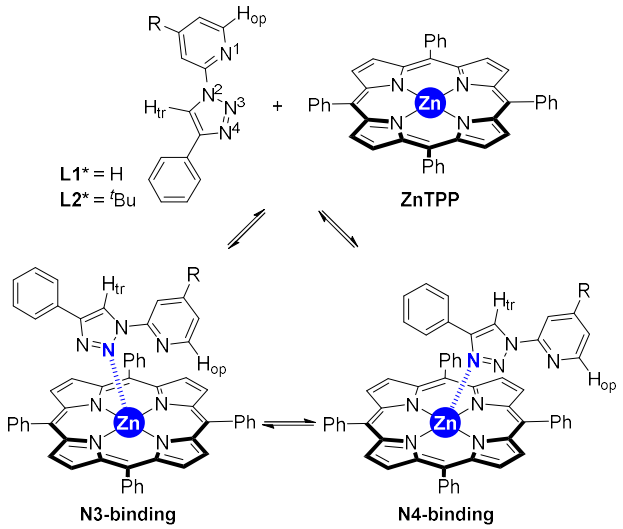

Scheme 4. Binding of triazolopyridine derivatives **L1*** (R = H) and **L2*** (R = ^{t}Bu) to unfunctionalized **ZnTPP** according to ^{1}H NMR spectroscopy studies.

The above-stated observations are in agreement with the triazolopyridine motif belonging to the supramolecular ligand binding to the zinc-porphyrin site *via* kinetically labile Zn···N interaction, which is enhanced by the presence of an electron-donating group such as 4-*tert*-butyl in the supramolecular ligand **L2** (**Scheme 5**). CPK modelling and previous literature on zinc-porphyrins appended with triazole fragments in the *ortho*-position of the *meso*-substituted phenyl rings[41] further indicate that the triazolopyridine fragment from the supramolecular ligands is highly rigid and hardly flexible to enable intramolecular binding to zinc. This leads only to intermolecular binding as feasible with an equilibrium involving four chemical species depending on the nitrogen atom that is involved in the binding to zinc as well as the top/bottom side-coordination (**Scheme 5**). The formation of higher oligomers or aggregates beyond dimers cannot be ruled out, but should be significantly less favored during the C-H bond borylation catalysis considering the low concentration of the catalyst in solution and the bulkiness of the substitution pattern in the triazolopyridine fragment (i.e. 4-*tert*-butyl group in **L2**). Moreover, it should be noted that the triazole protons (H_{tr}) from the supramolecular ligands resonate at high up-field shifts (δ = 5.28 ppm for **L2**) compared to the parent triazolopyiridine lacking a zinc-porphyrin (δ = 8.80 ppm for **L2***). Whether this is due to the zinc porphyrin current effect[41] or due to intermolecular binding as shown in **Scheme 5** or both effects simultaneously remains to be addressed.

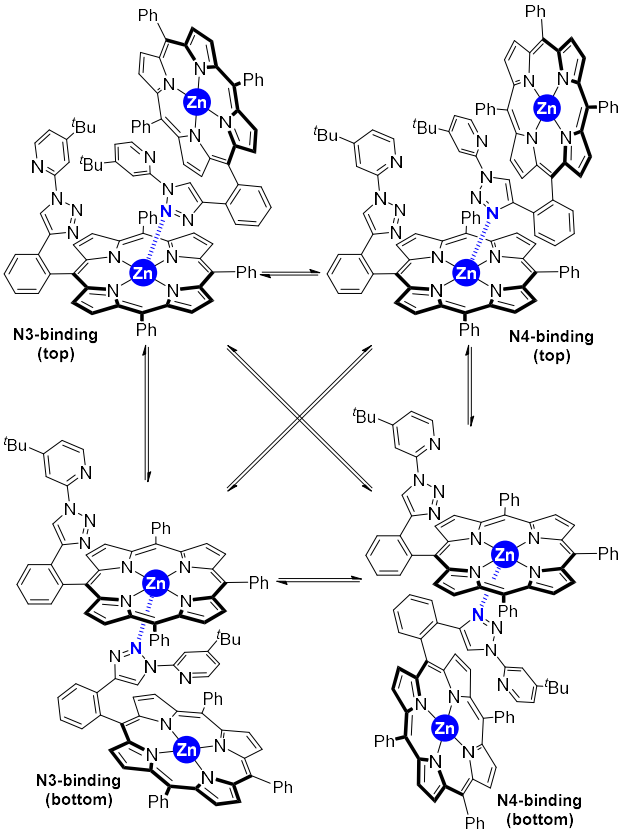

Scheme 5. Catalyst deactivation pathway *via* intermolecular binding of the triazolopyridine fragment to the zinc-porphyrin site from the supramolecular ligand **L2**.

Identification of the most reactive supramolecular catalyst. Having established several experimentally-assessed deactivation pathways that need to be circumvented in order to reach a reactive system for this supramolecular catalysis, we evaluated the supramolecular ligands **L3**-**L6** in the iridium-catalyzed C-H borylation of pyridine (**1a**) with B_2pin_2 (**Table 4**). At 80 °C and using 3 mol% of the *in situ* formed supramolecular iridium catalyst during 24 hours, the *para*- and *ortho*-methyl-substituted supramolecular ligands **L3** and **L4** performed equally well (**Table 4**, entries 1-2) as the unfunctionalized supramolecular ligand **L1** (**Table 3**, entry 1) with full conversion of starting material and similar ratios of mono- and bis-borylated products resulting from *meta*-C-H bond selectivity. On the other hand, and as it could be expected for electron-donating groups placed in the triazolopyridine fragment such as **L2** (*vide supra*), **L5**, which contains 4-methoxy substituent in *para*-position of the pyridine ring, enabled a modest 55% conversion of **1a** (**Table 4**, entry 3). The strong electron withdrawing trifluoromethoxy-substituted supramolecular ligand **L6** only converted 36% of the starting material (**Table 4**, entry 4). This is in agreement with the fact that the rate determining step (rds) of the iridium-catalyzed (hetero)aromatic C-H borylation with *N*,*N*-chelating type ligands is the oxidative addition of the C-H bond, largely favored by electron density enhancement on the iridium-coordinated ligand backbone.[17-19,30] To further explain the poor performance in catalysis of the methoxy-substituted **L5** versus their alkyl counterparts, we reasoned that the methoxy group in **L5** may bind to some extent in an intramolecular fashion to the zinc center of the molecular recognition

site according to CPK modelling, as similarly observed for oxophilic deactivation pathways involving water and methoxide anions (*vide supra*). Along these lines, raising the reaction temperature to 100 °C when employing the supramolecular ligands **L5** and **L6** led to full conversion of **1a** (**Table 4**, entries 5-6). The reactivity of the supramolecular ligands **L5** and **L6** is in stark contrast with that observed with the supramolecular ligand **L2** that does not lead to full conversion even at such high temperatures and beyond (*vide supra*). At full conversion, the ratio of mono- *versus* bis-borylation **2a** : **2aa** varied little (in the range 40 : 60 to 60 : 40) to establish any relevant trend between the supramolecular ligands **L1** (**Table 3**, entry 1) and **L3**-**L6** (**Table 4**, entries 1-2 and 5-6). Note that the ratio mono- *versus* bis-arylation was not affected at longer reaction times.

Table 4. Evaluation of the supramolecular ligands in the iridium-catalyzed *meta*-selective C-H borylation of pyridine.[a]

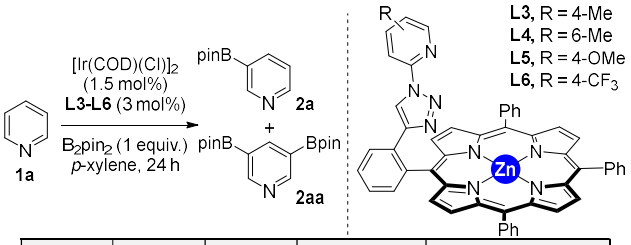

Entry	L	T (°C)	Conv.[b]	2a : 2aa (%)[c]
1	**L3**	80	>99 %	50 : 50
2	**L4**	80	>99 %	60 : 40
3	**L5**	80	55 %	84 : 16
4	**L6**	80	36 %	89 : 11
5	**L5**	100	>99 %	56 : 44
6	**L6**	100	>99 %	44 : 56

[a] Reaction conditions: pyridine (0.162 mmol), B_2pin_2 (0.162 mmol), $[Ir(COD)(Cl)]_2$ (1.5 mol%), **L** (3 mol%), *p*-xylene (1 mL), 24 h. [b] Conversion determined as pyridine consumption, the remaining % corresponds to unreacted pyridine starting material. [c] Ratio of borylated products determined by ^{1}HNMR and GC using *n*-dodecane as internal standard.

Notably, the regio-selectivity observed for the supramolecular iridium-catalyzed C-H bond borylation of the unfunctionalized pyridine **1a** was the same for any supramolecular ligand being tested. An excellent *meta*-selectivity (>99%) was obtained with no presence of the *ortho*- or *para*-borylated products. Consequently, the selectivity is determined exclusively by the high level of substrate pre-organization taking place within the secondary coordination sphere in which the *meta*-C-H bond from pyridine is brought at very close proximity of iridium to undergo C-H bond cleavage regardless of the nature of the iridium-coordinated triazolopyridine fragment. However, the reactivity is clearly controlled by the first coordination sphere at iridium as observed by kinetic studies using the most promising supramolecular ligands **L1**, **L3** and **L4**. For this kinetic evaluation, 3-methylpyridine (**1b**) was selected as substrate of choice since it only provides a single product resulting from *meta*-C-H borylation, namely **2b** (**Figure 4**). The main difference between these supramolecular ligands is the length of the incubation period for forming the catalytically active iridium species. At 80 °C, the unfunctionalized supramolecular ligand **L1** leads to a system in which the catalysis begins after 3 hours (red dashed line, **Figure 4**). This incubation period is reduced by more than half when using the methyl-substituted supramolecular ligands **L3** (1 hour incubation time, blue dashed line - **Figure 4**) and **L4** (1.5 hours incubation time, yellow dashed line - **Figure 4**). A superior reaction rate was found for the supramolecular ligand **L3** with almost full conversion reached in less than 6 hours at 80 °C (blue dashed line - **Figure 4**). The lower reaction rate found for the supramolecular ligand **L4** that contains an *ortho*-substituted methyl group in the triazolopyridine fragment indicates that the reactivity of the supramolecular catalyst is sensitive to steric effects at the first coordination sphere of the active iridium site. Considering the C-H activation being likely the rds (*vide supra*), steric hindrance appears to be detrimental for this reaction as it disfavors oxidative addition to some extent.

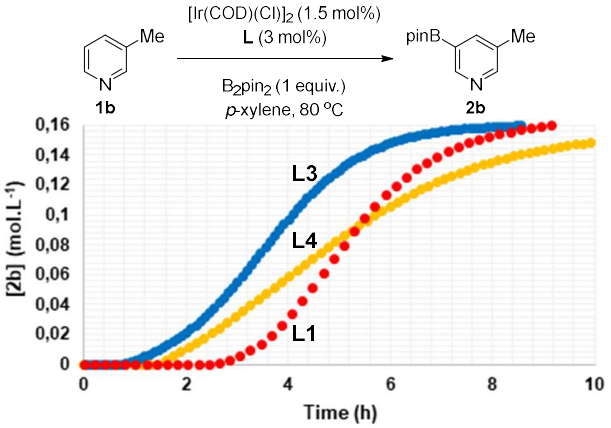

Figure 4. Kinetic evaluation (formation of product **2b** *versus* time) of the supramolecular ligands **L1** (red dashed line), **L3** (blue dashed line) and **L4** (yellow dashed line) in the iridium-catalyzed C-H borylation of 3-methylpyridine (**1b**).

Calculations. In order to better understand the origin of the reactivity observed and the absence of difference in the regioselectivity for all the supramolecular ligands being tested in the C-H borylation of pyridine, Density Functional Theory (DFT) calculations were carried out for the most energetically demanding elementary steps (**Table 5**), namely the oxidative addition C-H activation (A→ B, **Figure 5**) and the reductive elimination C-B bond-forming step (B → C, **Figure 6**) based on our previous computational work.[30] The reference zero energy corresponds to the neutral species [**L**Ir(COD)(Bpin)$_3$] that initially may form.[30] Analysing the **TS$_{AB}$**, it is possible to observe that electron donating group (EDG) in position 4 of the iridium-coordinated pyridyl group does not vary much the activation barrier energy (ΔΔG = +0.4 kcal/mol for **L2**, -0.2 kcal/mol for **L3**, -0.6 kcal/mol for **L5**). On the other hand, the presence of an electron withdrawing group (EWG) in the same position leads to a greater activation barrier energy (ΔΔG = +1.8 kcal/mol for **L6**), whereas a methyl in position 6 next to the nitrogen speed up the reaction (ΔΔG = -8.7 kcal/mol for **L4**). On the other hand, we looked at the C-B bond formation step to see whether modifying the substituents, the rds would have changed, and in this case, the **TS$_{BC}$** energies are in agreement with the experimental

conversions. The result also agrees well with the fact that the reductive elimination C-B bond-forming step is favoured at the *meta* position of the pyridine substrate as previously reported for the supramolecular ligand **L1**.[30] As shown in **Table 5**, TS_{BC} have been affected by the variation of the substituents, but not enough to produce a change of rds. In presence of EWG, the reductive elimination C-B bond formation step results to have a greater activation barrier energy (ΔΔG = +2.3 kcal/mol for **L6**). Alternatively, in presence of EDG the situation is more complex. In fact, a methyl group as substituent stabilized the TS of the process (ΔΔG = -1.0 kcal/mol for **L3**, ΔΔG = -2.1 kcal/mol for **L4**), while a *tert*-butyl group leads to the opposite (ΔΔG = +3.1 kcal/mol for **L2**). Overall, the rds of the reaction for **L2**-**L6** appears to be TS_{AB} except for **L4** that corresponds to the next TS_{BC}.

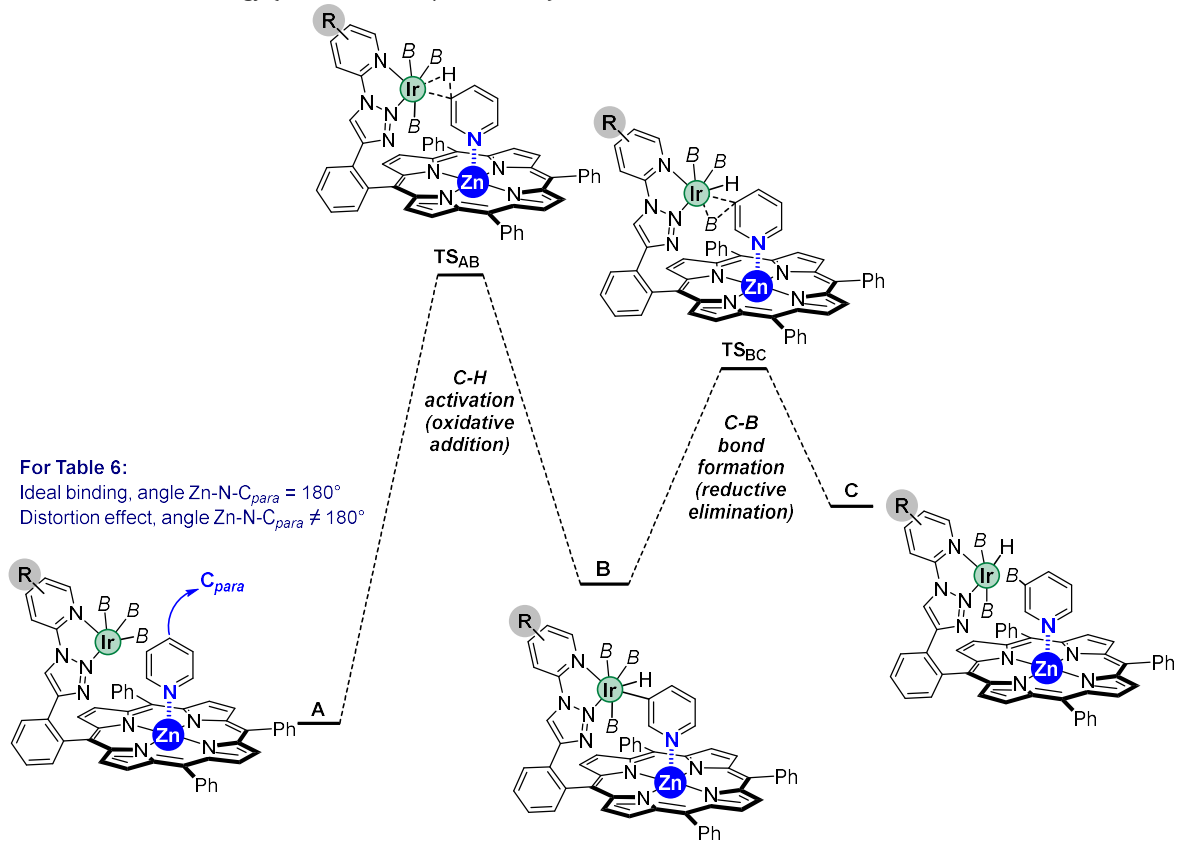

Figure 5. Qualitative energetic profile for the iridium-mediated *meta*-C-H activation (oxidative addition) step of pyridine and carbon-boron bond-forming (reductive elimination) step in *meta* position of pyridine with the supramolecular ligands developed in this study (see the quantitative computational data in **Table 5**).

Table 5. Computational data (in kcal/mol) regarding the stability of each intermediate and transition state involved in the oxidative addition C-H activation and the reductive elimination C-B bond-forming elementary steps.

Ligand	A	TS_{AB}	B	TS_{BC}
L1	1.4	33.7	8.4	27.1
L2	3.5	34.1	8.7	30.2
L3	2.3	33.5	8.1	26.1
L4	2.7	25.0	12.4	25.0
L5	1.5	33.1	8.2	30.2
L6	3.1	35.5	9.7	29.4

Aiming at explaining some general trends, we considered the correlations between the transition state energy barriers and steric/electronic descriptors related to the intermediate **A**, which is the sterically most congested one.[30] As shown in **Table 6** (and Table S2 in the Supporting Information) , there is a good correlation between TS_{BC} energies and the HOMO of intermediate **A**: the more stable this HOMO is, the lower the energy barrier appears to be. In addition, it is relevant to note that the highest distortion observed for the iridium intermediate **A** (Zn-N-C_{para} angle, **Figure 5** and **Table 6**) corresponds to the ligand **L2**, which features the lowest activity in catalysis from the series. This is an indirect proof that the substrate binding into **L2** at the iridium intermediate **A** is much more disfavoured compared to the other supramolecular ligands.

Table 6. Descriptors considered for the iridium intermediates **A** with the supramolecular ligands **L1**-**L6**.

L	Zn-N-C_{para} angle (**A**)[a]	HOMO (a.u.)	LUMO (a.u.)	η	V_{bur} (%)
L1	151.20°	-0.1860	-0.0916	0.0944	66.1
L2	147.99°	-0.1850	-0.0902	0.0948	69.5
L3	150.86°	-0.1857	-0.0915	0.0942	71.0
L4	151.01°	-0.1861	-0.0913	0.0948	67.8
L5	150.99°	-0.1848	-0.0900	0.0948	75.5
L6	149.65°	-0.1852	-0.0913	0.0939	78.5

[a] The Zn-N-C_{para} angle at the intermediate **A** stands for the deviation angle between the zinc-porphyrin molecular recognition site and the pyridine substrate; and it gives an approximation of distortion effects in the secondary coordination sphere (see details in **Figure 5**).

Non-covalent interaction (NCI) plots were calculated and analysed for the iridium intermediates **A** formed from each supramolecular ligand **L1**-**L6** (Figure S45 in the Supporting Information). Besides the Zn···N interaction, all the intermediates **A** have two additional non-covalent interactions in common: one between the pyridine substrate and the iridium-coordinated triazolopyridine moiety *via* π- π interactions, and a second one between one of the *meso*-located porphyrinic phenyl groups and one of the methyl groups from an iridium-ligated boronpinacolato group (see **Figure 6** for the case of **L3**). The only interaction that changes is the one between the substituents around the iridium centre and *meso*-located phenyl groups of the porphyrin backbone because of the different shape and size of the substituent. Moreover, in the case of **L4** there is a non-covalent interaction between the methyl group from the triazolopyridine site and the methylene protons from the boryl group, which explains why the energy barriers for this system are the lowest of the series.

Furthermore, we calculated the NCI for the $\mathbf{TS_{AB}}$ (the transition state of the oxidative addition C-H bond activation elementary step) involving each supramolecular ligand **L1**-**L6** (Figure S46 in the Supporting Information). In these cases, there are two important non-covalent interactions: the interaction between one of the methylene groups of the boronpinacolato group and the pyridine substrate, and the interaction between the hydrogens of one of the *meso*-located porphyrinic phenyl groups and the hydrogens from the iridium-coordinated triazolopyridine moiety *via* a T-shape conformation. It can be noted that the iridium-hydride proton appears to be at close proximity to one of the hydrogen atoms from a meso-phenyl ring. The additional interactions that were present in the intermediates **A** were lost in $\mathbf{TS_{AB}}$. Finally, in $\mathbf{TS_{BC}}$ (the transition state of borylation, Figure S47 in the Supporting Information). The most important non-covalent interaction according to NCI plots was found to be the one between one of the *meso*-located porphyrinic phenyl groups and one of the methyl groups from an iridium-ligated boronpinacolato unit similar to that found for intermediates **A**. The interaction between the pyridine substrate and the iridium-coordinated triazolopyridine moiety, and that between the triazolpyridine substituents and the porphyrinic phenyl groups are present but significantly less strong because the groups are more wide apart to each other. Overall, the role of the supramolecular ligands **L1**-**L6** in the key intermediates and transition states is manifold. On one hand, the supramolecular ligands bring the pyridine substrate in a specific conformation close to the active site to reach *meta*-selectivity *via* remote kinetically labile Zn···N interaction. On the other hand, the supramolecular ligands are involved in additional sort of remote non-covalent interactions thanks to the highly constrained environment in the secondary coordination sphere even beyond the molecular recognition site. A representative overview of the action mode of these supramolecular catalysts is highlighted in **Figure 6** for the most active system: the one derived from ligand **L3**. These computational insights point out the importance of considering deactivation pathways beyond the main catalytic cycle difficult to predict beforehand.

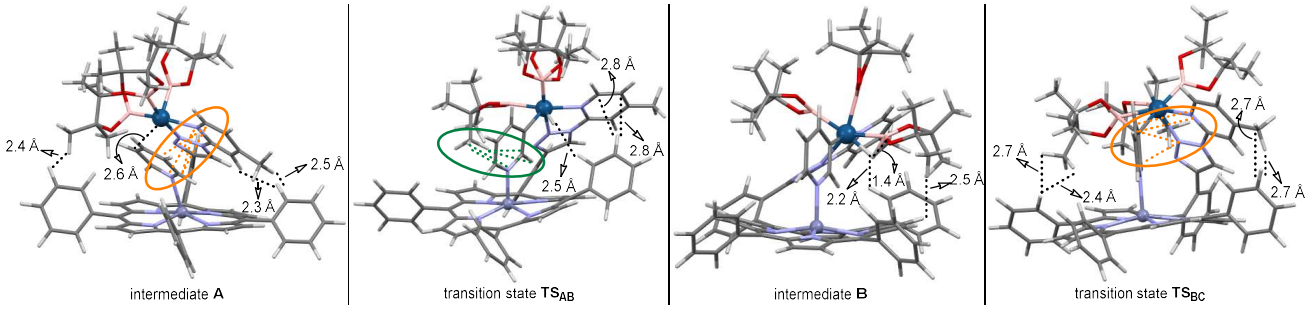

Figure 6. 3D structures of the intermediates and transition states involving the supramolecular ligand **L3** highlighting a number of non-covalent interactactions (orange dashed lines indicate interactions with distances inferior to 3.2 Å which are indicative of π- π interactions, green dashed lines indicate interactions with distances ca. 2.7-2.8 Å).

Boosting the selective supramolecular iridium-catalyzed *β*-selective C-H borylation and substrate scope. Next, we envisioned the use of catalytic amounts of additives such as 2,6-lutidine and HBpin, respectively, because they are known to promote the formation of the catalytically active iridium tris-boryl species in some cases.[21a] The supramolecular ligand **L3**, which features a 4-methyl substitution pattern, was selected considering its higher performance over the other ligands and the iridium-catalyzed C-H borylation of **1b** was monitored over time in the presence of catalytic amounts of each additive (**Figure 7**). The reaction in the presence of 2,6-lutidine (4 mol%) slowed down the reaction (red dashed line, **Figure 7**) compared to the catalysis performed in the absence of any additive (blue dashed line, **Figure 7**). No borylation occurred in the 2,6-lutidine additive in accordance to what is observed using 2-methylpyridine as the substrate (*vide infra*). Importantly, the catalysis carried out in the presence of HBpin (4 mol%) led to an almost negligible incubation period at 80 °C (green dashed line, **Figure 7**), similar to previous observations by the Hartwig group on iridium-catalyzed C-H borylations of aromatic groups.[28f] Under this reaction conditions, only trace amounts of borylation at the solvent were identified. For the most unfavorable scenario (5% of borylation at the solvent), this corresponds to an exceptional selectivity factor *S* ca. 10^3 when compared to the pyridine selectivity over the aromatic solvents being used either toluene (S_{pyr} = 1149) or *para*-xylene (S_{pyr} = 991).[42] These values correspond to a four-fold increase in the substrate selectivity compared to our previous report.[26] On the other hand, substantial ligand degradation was evidenced and not more than 20% of pure ligand could be recovered after the catalysis. Consequently, further studies should have to be carried out to further understand these decomposition pathways at the ligand which make likely involve borylation at the supramolecular ligand.

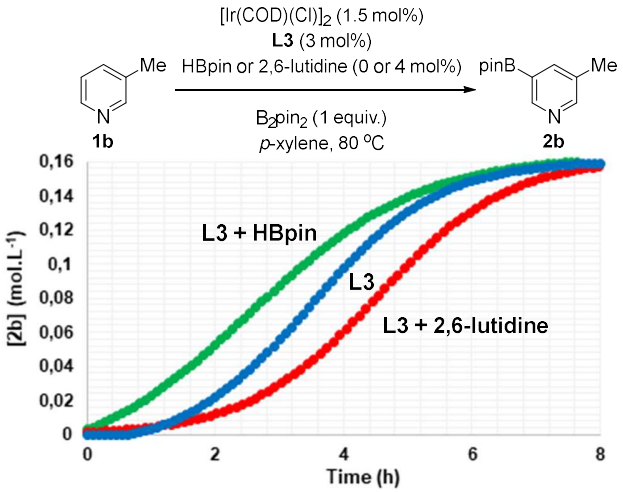

Figure 7. Kinetic evaluation (formation of product **2b** *versus* time) of the supramolecular ligand **L3** in the presence (HBpin - green dashed line-, 2,6-lutidine -red dashed line-) or absence of additive (blue dashed line) for the iridium-catalyzed C-H borylation of 3-methylpyridine (**1b**).

Importantly, it was possible to reduce the reaction time to only 2 hours with 99% formation of the *meta*-borylated product **2b** by increasing the reaction temperature to 100 °C in the presence of 4 mol% of HBpin and 3 mol% of the supramolecular iridium catalyst (**Scheme 6**). Compared to our previously reported methodology,[26] the reaction time was notably reduced from 9 to 2 hours for the formation of **2b**. Such observation was a general trend as regards of the substrate scope evaluation reported in **Scheme 6** with carefully optimized reaction time for each starting material. By using the optimal reaction conditions with **L3**, a variety of *meta*-substituted pyridine derivatives (**1c**-**1j**) with different steric and electronic properties selectively underwent iridium-catalyzed C-H bond borylation in very short reaction times (from 2 to 5.5 hours) affording the corresponding *meta*-borylated products **2c**-**2j** in excellent yields. For instance, the superb reactivity encountered for this supramolecular iridium catalyst was exemplified with the borylation of the bromo- and methoxy-containing pyridine substrates **1e** and **1f**, respectively. Whereas the previous methodology required 24 hours to get full conversion,[26] the present one affords the same selective products in only 3.5 and 2 hours, respectively. An even much clearer example concerns the fluorinated compound **2h**, which was obtained previously in a modest 50% yield in 24 hours,[26] whilst the current methodology affords it in 99% yield in less than 6 hours. Importantly, 3-phenylpyridine **1i** was selectively borylated at the heteroaromatic pyridine ring and not in the aromatic phenyl ring, additionally supporting the fact that kinetically labile Zn···N interactions are at play for controlling not only the regioselectivity but also the site-selectivity of the iridium-catalyzed C-H bond borylation. The highly selective formation of carbonyl-containing *meta*-borylated products **2g** and **2j** further indicates that the supramolecular catalysis is compatible with even potentially competing *ortho*-directing groups such as ketone and esters.[5-7] Limitations in the catalysis were encountered by using iodide, carboxylic acid and primary amide functional groups (**Scheme 6**). As shown previously for the supramolecular ligand **L1**,[26] the catalysis was sensitive to steric shields with a lack of reactivity found for *ortho*- and *para*-substituted pyridines (**Scheme 6**). At 120 °C, we noted that the iridium catalyst started to borylate the *p*-xylene solvent and the B_2pin_2 decomposed significantly under our reaction conditions. Other borylating reagents such as HBpin, bis(catecholato)diboron and bis(neopentyl glycolato)diboron were evaluated although leading to low levels of activity when compared to B_2pin_2.[43] Overall, this further supports the complexity of the catalytic system, which require both a well-defined geometry regarding the substrate-to-ligand interaction as well as the non-covalent interactions between the iridium-ligated Bpin moiety and the *meso*-phenyl rings from the porphyrin backbone beyond the molecular recognition site.

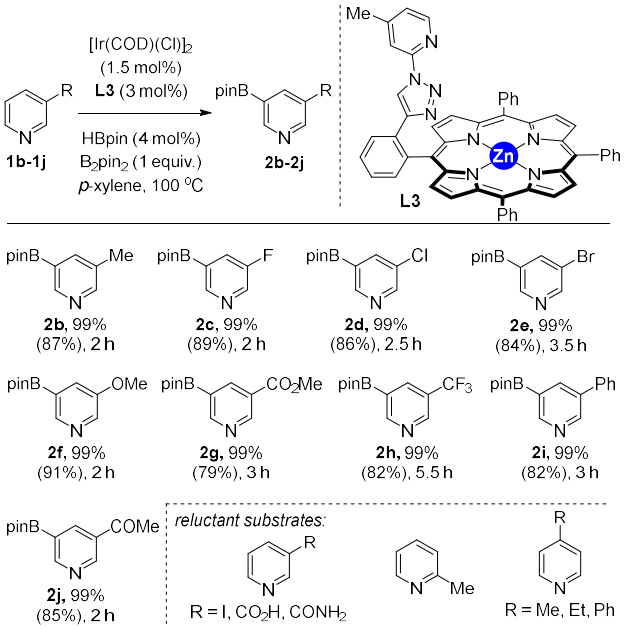

Scheme 6. Substrate evaluation for the supramolecular iridium-catalyzed C-H bond *meta*-borylation of pyridine derivatives using ligand **L3** (yields are determined by GC analysis and isolated yields are shown in brackets).[44]

In view to address the reactivity for other nitrogen-containing heterocycles, we turned our attention to imidazoles (**Scheme 7**).[45] The supramolecular iridium-catalyzed C-H borylation using ligand **L3** in the presence of B_2pin_2 and catalytic amounts of HBpin enabled the functionalization of *N*-methylimidazole (**1k**) in 5 hours at 100 °C leading selectively to the *β*-borylated product **2k** in 99% selectivity and 90% isolated yield (**Scheme 7**).[31] Such reactivity strikingly contrasts with the previously reported methodology that required 24 hours of reaction time.[26] As it is the case for pyridine derivatives, the borylation in the imidazole backbone takes place in the C-H bond located at a distance of four chemical bonds apart from the substrate-recognition site of the catalyst. In addition, attempts to perform iridium-catalyzed C-H borylation with **1k** employing **dtbpy** ligand with or without **ZnTPP** instead of **L3** revealed unsuccessful under our reaction conditions (<10% conversion of **1k**).[31] Such observations indicate that the substrate pre-organization between the active site and the binding of the substrate to the molecular recognition site *via* kinetically labile Zn···N interactions is mandatory to reach the observed activity and selectivity for the imidazole backbone. *N*-benzyl substituted imidazole **1l** afforded the corresponding *β*-borylated product **2l** in 92% yield with no borylation being ob-

served at the aromatic group, which is a relevant site-selectivity case of study. The catalysis was also compatible and selective for C2-substituted imidazoles as shown by the formation of the *β*-borylated product **2m** in 85% yield after only 5 hours reaction time. Note that unfunctionalized *N*-H imidazole, *N*-H pyrrole and *N*-alkyl pyrroles were unreactive for the supramolecular iridium-catalyzed C-H borylation.

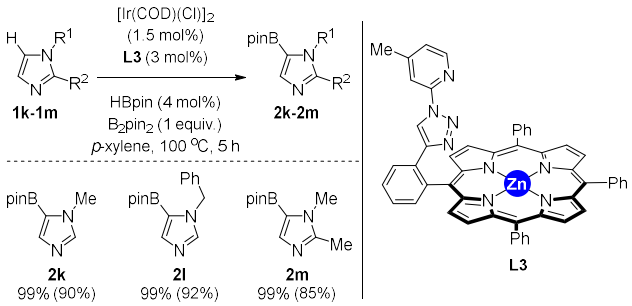

Scheme 7. *β*-selective supramolecular iridium-catalyzed C-H bond borylation of *N*-functionalized imidazoles using ligand **L3** (yield is determined by GC analysis and isolated yield is shown in brackets).[44]

CONCLUSION

In summary, the overall reported data indicate that the supramolecular iridium catalyst formed when using ligand **L3** offers a suitable balance of steric and electronic effects in order to reach *β*-selective C-H bond borylations at pyridines and imidazoles, while significantly avoiding several catalyst deactivation pathways experimentally identified. Interestingly, with this supramolecular approach, the selectivity is fully compatible with the reactivity at high temperatures and short reaction times, which is a major challenge in transition metal catalysis.[46] The main reason that explains the excellent selectivity is the optimal distance between the active site and the substrate recognition site in the secondary coordination sphere of the catalyst, which is the exclusive parameter that determines the regioselectivity of the borylation for pyridines. In the case of imidazoles, the reactivity is increased by the enhanced effective molarity of the substrates around the active site thanks to the molecular recognition site. On the other hand, the activity of the catalyst is strongly dependent by the first coordination sphere around iridium, which is upgraded by the use of catalytic amounts of HBpin as additive at 100 °C that further enables almost negligible incubation period for catalyst activation, which is so far unprecedented in iridium-catalyzed C-H bond borylation of heteroaromatic groups. The supramolecular catalysis herein disclosed represents a unique example of extremely fast and selective C-H bond functionalizations by exploiting remote, kinetically labile Zn···N interactions.[20] The benefits of exploiting kinetically labile interactions between Lewis base-containing substrates and metalloporphyrins containing peripherally located active sites may give rise to new tools to control activity and selectivity in challenging transformations.[47] In addition, thanks to in-depth computational calculations it was possible to rationalize the reactivity encountered in this supramolecular catalysis in which additional secondary non-covalent interactions beyond the molecular recognition site are at play. This contribution demonstrates the power of supramolecular catalysts featuring rationally-designed substrate-recognitions sites for the development of extremely active and selective catalytic systems.[48]

AUTHOR INFORMATION

Corresponding Author

Rafael Gramage-Doria, Univ Rennes, CNRS, ISCR-UMR6226, F-35000 Rennes (France); orcid.org/0000-0002-0961-4530; e-mail: rafael.gramage-doria@univ-rennes1.fr

Albert Poater, Institut de Química Computacional i Catàlisi, Departament de Química, Universitat de Girona, c/Mª Aurèlia Capmany 69, 17003 Girona, Catalonia, Spain; orcid.org/0000-0002-8997-2599; e-mail: albert.poater@udg.edu

Authors

Jonathan Trouvé, Univ Rennes, CNRS, ISCR-UMR6226, F-35000 Rennes (France)
Purushothaman Rajeshwaran, Univ Rennes, CNRS, ISCR-UMR6226, F-35000 Rennes (France)
Michele Tomasini, Institut de Química Computacional i Catàlisi, Departament de Química, Universitat de Girona, c/Mª Aurèlia Capmany 69, 17003 Girona, Catalonia, Spain; orcid.org/0000-0002-1366-1401.
Antoine Perennes, Univ Rennes, CNRS, ISCR-UMR6226, F-35000 Rennes (France)
Thierry Roisnel, Univ Rennes, CNRS, ISCR-UMR6226, F-35000 Rennes (France)

Notes

The authors declare no competing financial interest.

ASSOCIATED CONTENT

Supporting Information

The Supporting Information is available free of charge at https://pubs.acs.org/doi/XXX.

Experimental details for the preparation of supramolecular ligands, supramolecular binding studies, catalytic experiments and details on isolation and characterization of the reaction products.

Accession Codes

CCDC 2214527 contains the supplementary crystallographic data for this paper. These data can be obtained free of charge via www.ccdc.cam.ac.uk/data_request/cif, or by emailing data_request@ccdc.cam.ac.uk, or by contacting The Cambridge Crystallographic Data Centre, 12 Union Road, Cambridge CB2 1EZ, UK; fax: +44 1223 336033.

ACKNOWLEDGMENTS

The CNRS, University of Rennes 1, Fondation Rennes 1 and Agence Nationale de la Recherche (ANR-19-CE07-0039) are acknowledged for financial support. A.P. is a Serra Húnter Fellow and ICREA Academia Prize 2019. A.P. thanks the Spanish Ministerio de Ciencia e Innovación for project PID2021-127423NB-I00 and the Generalitat de Catalunya for project 2021SGR623.

REFERENCES

(1) (a) Noyori, R. Synthesizing our future. *Nat. Chem.* **2009**, *1*, 5–6. (b) Sanderson, K. Chemistry: It's not easy being green. *Nature* **2011**, *469*, 18–20.

(2) Sheldon, R. A. Fundamentals of green chemistry: efficiency in reaction design. *Chem. Soc. Rev.* **2012**, *41*, 1437–1451.

(3) (a) van Leeuwen, P. W. N. M. *Homogeneous Catalysis: Understanding the Art*, Kluwer, Dordrecht, **2004**. (b) Kamer, P. C. J.; van Leeuwen, P. W. N. M. *Phosphorus(III) Ligands in Homogeneous Catalysis: Design and Synthesis*, Wiley-VCH, Weinheim, **2012**

(4) (a) Hartwig, J. F. *Organotransition Metal Chemistry: From Bonding to Catalysis*, University Science Books, Sausalito, **2009**. (b)

de Meijere, A.; Braese, S.; Oestreich, M. *Metal-Catalyzed Cross-Coupling Reactions and More*, Wiley-VCH, Weinheim, **2014**.

(5) (a) Yu, J.-Q.; Shi, Z. *C-H Activation in Topics in Current Chemistry*, Springer, Berlin, **2010**. (b) Shang, R.; Ilies, L.; Nakamura, E. Iron-Catalyzed C–H Bond Activation. *Chem. Rev.* **2017**, *117*, 9086–9139. (c) Yang, Y.; Lan, J.; You, J. Oxidative C–H/C–H Coupling Reactions between Two (Hetero)arenes. *Chem. Rev.* **2017**, *117*, 8787–8863. (d) McMurray, L.; O'Hara, F.; Gaunt, M. J. Recent developments in natural product synthesis using metal-catalysed C–H bond functionalization. *Chem. Soc. Rev.* **2011**, *40*, 1885–1898. (e) Karimov, R. R.; Hartwig, J. F. Transition-Metal-Catalyzed Selective Functionalization of C(sp^3)-H Bonds in Natural Products. *Angew. Chem. Int. Ed.* **2018**, *57*, 4234–4241. (f) Yamaguchi, J.; Yamaguchi, A. D.; Itami, K. C-H bond functionalization: emerging synthetic tools for natural products and pharmaceuticals. *Angew. Chem. Int. Ed.* **2012**, *51*, 8960–9009. (g) Dalton, T.; Faber, T.; Glorius, F. C–H Activation: Toward Sustainability and Applications. *ACS Cent. Sci.* **2021,** *7*, 245–261. (h) Rogge, T.; Kaplaneris, N.; Chatani, N.; Kim, J.; Chang, S.; Punji, B.; Schafer, L. L.; Musaev, D. G.; Wencel-Delord, J.; Roberts, C. A.; Sarpong, R.; Wilson, Z. E.; Brimble, M. A.; Johansson, M. J.; Ackermann, L. C–H activation. *Nat. Rev. Methods Primers* **2021**, *1*, 43. (i) Jana, R.; Begam, H. M.; Dinda, E. The emergence of the C–H functionalization strategy in medicinal chemistry and drug discovery. *Chem. Commun.* **2021,** *57*, 10842-10866. (j) Guillemard, L.; Kaplaneris, N.; Ackermann, L.; Johansson, M. J. Late-stage C–H functionalization offers new opportunities in drug discovery. *Nat. Rev. Chem.* **2021**, **5**, 522–545.

(6) (a) Rej, S. ; Ano, Y.; Chatani, N. Bidentate Directing Groups: An Efficient Tool in C–H Bond Functionalization Chemistry for the Expedient Construction of C–C Bonds. *Chem. Rev.* **2020**, *120*, 1788–1887. (b) Meng, G.; Lam, N. Y. S.; Lucas, E. L.; Saint- Denis, T. G.; Verma, P.; Chekshin, N.; Yu, J.-Q. Achieving Site-Selectivity for C–H Activation Processes Based on Distance and Geometry: A Carpenter's Approach, *J. Am. Chem. Soc.* **2020**, *142*, 10571–10591. (c) Zhu, R.-Y.; Farmer, M. E.; Chen, Y.-Q.; Yu, J.- Q. A Simple and Versatile Amide Directing Group for C-H Functionalizations. *Angew. Chem. Int. Ed.* **2016**, *55*, 10578–10599. (d) Davies, D. L.; Macgregor, S. A.; McMullin, C. L. Computational Studies of Carboxylate-Assisted C-H Activation and Functionalization at Group 8-10 Transition Metal Centers. *Chem. Rev.* **2017**, *117*, 8649–8709. (e) Ackermann, L. Carboxylate-Assisted Transition-Metal-Catalyzed C–H Bond Functionalizations: Mechanism and Scope. *Chem. Rev.* **2011**, *111*, 1315–1345. (f) Cernak, T.; Dykstra, K. D.; Tyagarajan, S.; Vachalb, P.; Krskab, S. W. The medicinal chemist's toolbox for late stage functionalization of drug-like molecules. *Chem. Soc. Rev.* **2016**, *45*, 546–576. (g) Hartwig, J. F. Evolution of C–H Bond Functionalization from Methane to Methodology. *J. Am. Chem. Soc.* **2016**, *138*, 2–24. (h) Sinha, S. K.; Guin, S.; Maiti, S.; Biswas, J. P.; Porey, S.; Maiti, D. Toolbox for Distal C–H Bond Functionalizations in Organic Molecules. *Chem. Rev.* **2022**, *122*, 5682–5841.

(7) (a) Sambiagio, C.; Schönbauer, D.; Blieck, R.; Dao-Huy, T.; Pototschnig, G.; Schaaf, P.; Wiesinger, T.; Zia, M. F.; Wencel-Delord, J.; Besset, T.; Maes, B. U. W.; Schnürch, M. A comprehensive overview of directing groups applied in metal-catalysed C–H functionalisation chemistry. *Chem. Soc. Rev.* **2018**, *47*, 6603–6743. (b) Engle, K. M.; Mei, T.-S.; Wasa, M.; Yu, J.-Q. Weak Coordination as a Powerful Means for Developing Broadly Useful C–H Functionalization Reactions. *Acc. Chem. Res.* **2012**, *45*, 788–802.

(8) (a) Kuhl, N.; Hopkinson, M. N.; Wencel-Delord, J.; Glorius, F. Beyond Directing Groups: Transition-Metal-Catalyzed C-H Activation of Simple Arenes. *Angew. Chem. Int. Ed.* **2012**, *51*, 10236–10254. (b) Della Ca, N.; Fontana, M.; Motti, E.; Catellani, M. Pd/Norbornene: A Winning Combination for Selective Aromatic Functionalization via C–H Bond Activation. *Acc. Chem. Res.* **2016**, *49*, 1389–1400. (c) Lichosyt, D.; Zhang, Y.; Hurej, K.; Dydio, P. Dual-catalytic transition metal systems for functionalization of unreactive sites of molecules. *Nat. Catal.* **2019**, *2*, 114–122. (d) Hartwig, J. F.; Larsen, M. A. Undirected, Homogeneous C–H Bond Functionalization: Challenges and Opportunities. *ACS Cent. Sci.* **2016**, *2*, 281–292.

(9) Bisht, R.; Haldar, C.; Hassan, M. M. M.; Hoque, M. E.; Chaturvedi, J.; Chattopadhyay, B. Metal-catalysed C–H bond activation and borylation. *Chem. Soc. Rev.* **2022,** *51*, 5042–5100.

(10) (a) Hartwig, J. F. Borylation and Silylation of C–H Bonds: A Platform for Diverse C–H Bond Functionalizations. *Acc. Chem. Res.* **2012,** *45*, 864–873. (b) Ros, A.; Fernandez, R.; Lassaletta, J. M. Functional group directed C–H borylation. *Chem. Soc. Rev.* **2014**, *43*, 3229–3243. (c) Hall, D. G. Boronic Acids. *Preparation, Applications in Organic Synthesis*, Wiley-VCH, Weinheim, **2011**. (d) Neeve, E. C.; Geier, S. J.; Mkhalid, I. A. I.; Westcott, S. A.; Marder, T. B. Diboron(4) Compounds: From Structural Curiosity to Synthetic Workhorse. *Chem. Rev.* **2016**, *116*, 9091–9161. (e) Wang, M.; Shi, Z. Methodologies and Strategies for Selective Borylation of C–Het and C–C Bonds. *Chem. Rev.* **2020**, *120*, 7348–7398.

(11) (a) Wen, J.; Wang, D.; Qian, J.; Wang, D.; Zhu, C.; Zhao, Y.; Shi, Z. Rhodium-Catalyzed P^{III}-Directed *ortho*-C–H Borylation of Arylphosphines. *Angew. Chem. Int. Ed.* **2019**, *58*, 2078–2082. (b) Tanaka, J.; Nagashima, Y.; Nagashima, Y.; Dias, A. J. A.; Tanaka, K. Photo-Induced *ortho*-C–H Borylation of Arenes through In Situ Generation of Rhodium(II) Ate Complexes. *J. Am. Chem. Soc.* **2021**, *143*, 11325–11331.

(12) Furukawa, T.; Tobisu, M.; Chatani, N. C–H Borylation by Platinum Catalysis. *Bull. Chem. Soc. Jpn.* **2017,** *90*, 332–342.

(13) (a) Obligacion, J. V.; Semproni, S. P.; Chirik, P. J. Cobalt-Catalyzed C–H Borylation. *J. Am. Chem. Soc.* **2014**, *136*, 4133–4136. (b) Obligacion, J. V.; Semproni, S. P.; Pappas, I.; Chirik, P. J. Cobalt-Catalyzed C(sp2)-H Borylation: Mechanistic Insights Inspire Catalyst Design. *J. Am. Chem. Soc.* **2016**, *138*, 10645–10653. (c) Pabst, T. P.; Chirik, P. J. Development of Cobalt Catalysts for the *meta*-Selective C(sp^2)–H Borylation of Fluorinated Arenes. J. Ame. Chem. Soc. **2022,** *144*, 6465–6474. (d) Ren, H.; Zhou, Y.-P.; Bai, Y.; Cui, C.; Driess, M. Cobalt-Catalyzed Regioselective Borylation of Arenes: N-Heterocyclic Silylene as an Electron Donor in the Metal-Mediated Activation of C–H Bonds. *Chem. Eur. J.* **2017,** *23*, 5663–5667.

(14) (a) Furukawa, T.; Tobisu, M.; Chatani, N. Nickel-Catalyzed Borylation of Arenes and Indoles via C-H Bond Cleavage. *Chem. Commun.* **2015**, *51*, 6508–6511. (b) Tian, Y.-M.; Guo, X.-N.; Wu, Z.; Friedrich, A.; Westcott, S. A.; Braunschweig, H.; Radius, U.; Marder, T. B. Ni-Catalyzed Traceless, Directed C3-Selective C–H Borylation of Indoles. *J. Am. Chem. Soc.* **2020**, *142*, 13136–13144.

(15) (a) Luo, Y.; Jiang, S.; Xu, X. Yttrium-Catalyzed *ortho*-Selective C–H Borylation of Pyridines with Pinacolborane. *Angew. Chem. Int. Ed.* **2022**, *61*, e202117750. (b) Rothbaum, J. O.; Motta, A.; Kratish, Y.; Marks, T. J. Chemodivergent Organolanthanide-Catalyzed C–H α-Mono-Borylation of Pyridines. *J. Am. Chem. Soc.* 2022, *144*, 17086–17096. (c) Q. Sun, Y. Luo, X. Xu, *Synlett* **2022**, *33*, 1961–1967.

(16) (a) Mkhalid, I. A. I.; Barnard, J. H.; Marder, T. B.; Murphy, J. M.; Hartwig, J. F. C–H Activation for the Construction of C–B Bonds. *Chem. Rev.* **2010,** *110*, 890–931. (b) Fernandez, E. Iridium-Catalyzed Undirected Homogeneous C–H Borylation Reaction. *Top. Organomet. Chem.* **2020**, *69*, 207-225. (c) Kuleshova, O.; Asako, S.; Ilies, L. Ligand-Enabled, Iridium-Catalyzed *ortho*-Borylation of Fluoroarenes. *ACS Catal.* **2021**, *11*, 5968–5973. (d) Hoque, M. E.; Hassan, M. M. M.; Chattopadhyay, B. Remarkably Efficient Iridium Catalysts for Directed C(sp^2)–H and C(sp^3)–H Borylation of Diverse Classes of Substrates. *J. Am. Chem. Soc.* 2021, **143**, 5022–5037. (e) Chang, W.; Chen, Y.; Lu, S.; Jiao, H.; Wang, Y.; Zheng, T.; Shi, Z.; Han, Y.; Lu, Y.; Wang, Y.; Pan, Y.; Yu, J.-Q.; Houk, K. N.; Liu, F.; Liang, Y. Computationally designed ligands enable tunable borylation of remote C–H bonds in arenes. *Chem* **2022,** *8*, 1775–1788.

(17) (a) Su, B.; Hartwig, J. F. Development of Chiral Ligands for the Transition-Metal-Catalyzed Enantioselective Silylation and Borylation of C–H Bonds. *Angew. Chem. Int. Ed.* **2022,** *61,* e202113343. (b) Xu, L.; Wang, G.; Zhang, S.; Wang, H.; Wang, L.; Liu, L.; Jiao, J.; Li, P. Recent advances in catalytic C–H borylation reactions. *Tetrahedron* **2017**, *73*, 7123-7157. (c) Xue, X.-S.; Ji, P.; Zhou, B.; Cheng, J.-P. The Essential Role of Bond Energetics in C–H Activation/Functionalization. *Chem. Rev.* **2017**, *117*, 8622–8648. (d)

Larsen, M. A.; Oeschger, R. J.; Hartwig, J. F. Effect of Ligand Structure on the Electron Density and Activity of Iridium Catalysts for the Borylation of Alkanes. *ACS Catal.* **2020**, *10*, 3415–3424. (e) Larsen, M. A.; Wilson, C. V.; Hartwig, J. F. Iridium-Catalyzed Borylation of Primary Benzylic C–H Bonds without a Directing Group: Scope, Mechanism, and Origins of Selectivity. *J. Am. Chem. Soc*. **2015**, *137*, 8633–8643. (f) Oeschger, R.; Su, B.; Yu, Y.; Ehinger, C.; Romero, E.; He, S.; Hartwig, J. Diverse functionalization of strong alkyl C–H bonds by undirected borylation. *Science* **2020,** *368*, 736-741.

(18) (a) Ishiyama, T.; Takagi, J.; Ishida, K.; Miyaura, N.; Anastasi, N. R.; Hartwig, J. F. Mild Iridium-Catalyzed Borylation of Arenes. High Turnover Numbers, Room Temperature Reactions, and Isolation of a Potential Intermediate. *J. Am. Chem. Soc.* **2002**, *124*, 390–391. (b) Ishiyama, T.; Takagi, J.; Hartwig, J. F.; Miyaura, N. A stoichiometric aromatic C-H borylation catalyzed by iridium(i)/2,2'-bipyridine complexes at room temperature. *Angew. Chem. Int. Ed.* **2002**, *41*, 3056–3058. (c) Ishiyama, T.; Nobuta, Y.; Hartwig, J. F.; Miyaura, N. Room temperature borylation of arenes and heteroarenes using stoichiometric amounts of pinacolborane catalyzed by iridium complexes in an inert solvent. *Chem. Commun.* **2003**, 2924–2925.

(19) (a) Liskey, C. W.; Wei, C. S.; Pahlsa, D. R.; Hartwig, J. F. Pronounced effects of substituents on the iridium-catalyzed borylation of aryl C–H bonds. *Chem. Commun.* **2009**, 5603–5605. (b) Oeschger, R. J.; Larsen, M. A.; Bismuto, A.; Hartwig, J. F. Origin of the Difference in Reactivity between Ir Catalysts for the Borylation of C–H Bonds. *J. Am. Chem. Soc.* **2019**, *141*, 16479–16485.

(20) (a) Pandit, S.; Maiti, S.; Maiti, S. Noncovalent interactions in Ir-catalyzed remote C–H borylation: a recent update. *Org. Chem. Front.* **2021**, *8*, 4349–4358. (b) Zou, X.; Xu, S. Recent Progress in Iridium-Catalyzed Remote Regioselective C-H Borylation of (Hetero)Arenes. *Chin. J. Org. Chem.* **2021**, *41*, 2610–2620. (c) Bai, S.-T.; Bheeter, C. B.; Reek, J. N. H. Hydrogen Bond Directed *ortho*-Selective C–H Borylation of Secondary Aromatic Amides. *Angew. Chem. Int. Ed.* **2019**, *58*, 37, 13039-13043. (d) Kuninobu, Y.; Ida, H.; Nishi, M.; Kanai, M. A *meta*-selective C-H borylation directed by a secondary interaction between ligand and substrate. *Nat. Chem.* **2015**, *7*, 712–717. (e) Wang, J.; Torigoe, T.; Kuninobu, Y. Hydrogen-Bond-Controlled Formal *Meta*-Selective C–H Transformations and Regioselective Synthesis of Multisubstituted Aromatic Compounds. *Org. Lett.* **2019**, *21*, 1342–1346. (f) Lu, X.; Yoshigoe, Y.; Ida, H.; Nishi, M.; Kanai, M.; Kuninobu, Y. Hydrogen Bond-Accelerated *meta*-Selective C–H Borylation of Aromatic Compounds and Expression of Functional Group and Substrate Specificities. *ACS Catal.* **2019**, *9*, 1705–1709. (g) Davis, H. J.; Mihai, M. T.; Phipps, R. J. Ion Pair-Directed Regiocontrol in Transition-Metal Catalysis: A Meta-Selective C–H Borylation of Aromatic Quaternary Ammonium Salts. *J. Am. Chem. Soc.* **2016**, *138*, 12759–12762. (h) Lee, B.; Mihai, M. T.; Stojalnikova, V.; Phipps, R. J. Ion-Pair-Directed Borylation of Aromatic Phosphonium Salts. *J. Org. Chem.* **2019**, *84*, 13124 –13134. (j) Mihai, M. T.; Davis, H. J.; Genov, G. R.; Phipps, R. J. Ion Pair-Directed C–H Activation on Flexible Ammonium Salts: *meta*-Selective Borylation of Quaternized Phenethylamines and Phenylpropylamines. *ACS Catal.* **2018**, *8*, 3764–3769. (i) Hoque, M. E.; Bisht, R.; Haldar, C.; Chattopadhyay, B. Noncovalent Interactions in Ir-Catalyzed C–H Activation: L-Shaped Ligand for *Para*-Selective Borylation of Aromatic Esters. *J. Am. Chem. Soc.* **2017**, *139*, 7745–7748. (j) Bisht, R.; Hoque, M. E.; Chattopadhyay, B. Amide Effects in C–H Activation: Noncovalent Interactions with L-Shaped Ligand for meta Borylation of Aromatic Amides. *Angew. Chem. Int. Ed.* **2018**, *57*, 15762–15766.

(21) (a) Wright, J. S.; Scott, P. J. H.; Steel, P. G. Iridium-Catalysed C–H Borylation of Heteroarenes: Balancing Steric and Electronic Regiocontrol. *Angew. Chem. Int. Ed.* **2021,** *60*, 2796–2821. (b) Yang, Y.; Gao, Q.; Xu, S. Ligand-Free Iridium-Catalyzed Dehydrogenative ortho C–H Borylation of Benzyl-2-Pyridines at Room Temperature. *Adv. Synth. Catal.* **2018**, *361*, 858-862. (c) Murakami, K.; Yamada, S.; Kaneda, T.; Itami, K. C–H Functionalization of Azines. *Chem. Rev.* **2017**, *117*, 9302–9332.

(22) (a) Takagi, J.; Sato, K.; Hartwig, J. F.; Ishiyama, T.; Miyaura, N. Iridium-catalyzed C–H coupling reaction of heteroaromatic compounds with bis(pinacolato)diboron: regioselective synthesis of heteroarylboronates. *Tetrahedron Lett.* **2002**, *43*, 5649–5651. (b) Ishiyama, T.; Takagi, J.; Yonekawa, Y.; Hartwig, J. F.; Miyaura, N. Iridium-Catalyzed Direct Borylation of Five-Membered Heteroarenes by Bis(pinacolato)diboron: Regioselective, Stoichiometric, and Room Temperature Reactions. *Adv. Synth. Catal.* **2003**, *345*, 1103–1106. (c) Larsen, M. A.; Hartwig, J. F. Iridium-Catalyzed C–H Borylation of Heteroarenes: Scope, Regioselectivity, Application to Late-Stage Functionalization, and Mechanism. *J. Am. Chem. Soc.* **2014**, *136*, 4287–4299. (d) Sasaki, I.; Taguchi, J.; Hiraki, S.; Ito, H.; Ishiyama, T. Catalyst-Controlled Regiodivergent C-H Borylation of Multifunctionalized Heteroarenes by Using Iridium Complexes. *Chem. Eur. J.* **2015**, *21*, 9236–9241.

(23) (a) Yang, L.; Uemura, N.; Nakao, Y. *meta*-Selective C–H Borylation of Benzamides and Pyridines by an Iridium–Lewis Acid Bifunctional Catalyst. *J. Am. Chem. Soc.* **2019**, *141*, 7972–7979. (b) Yang, L.; Semba, K.; Nakao, Y. *para*-Selective C–H Borylation of (Hetero)Arenes by Cooperative Iridium/Aluminum Catalysis. *Angew. Chem. Int. Ed.* **2017**, *56*, 4853–4857.

(24) (a) Kallepalli, V. A.; Shi, F.; Paul, S.; Onyeozili, E. N.; Maleczka, R. E.; Smith, M. R. Boc groups as protectors and directors for Ir-catalyzed C-H borylation of heterocycles. *J. Org. Chem.* **2009**, *74*, 9199–9201. (b) Preshlock, S. M.; Plattner, D. L.; Maligres, P. E.; Krska, S. W.; Maleczka, R. E.; Smith, M. R. A Traceless Directing Group for C-H Borylation. *Angew. Chem. Int. Ed.* **2013**, *52*, 12915–12919.

(25) (a) Sadler, S. A.; Tajuddin, H.; Mkhalid, I. A. I.; Batsanov, A. S.; Albesa-Jove, D.; Cheung, M. S.; Maxwell, A. C.; Shukla, L.; Roberts, B.; Blakemore, D. C.; Lin, Z.; Marder, T. B.; Steel, P. G. Iridium-catalyzed C–H borylation of pyridines. *Org. Biomol. Chem.* **2014**, *12*, 7318–7327. (b) Tajuddin, H.; Harrisson, P.; Bitterlich, B.; Collings, J. C.; Sim, N.; Batsanov, A. S.; Cheung, M. S.; Kawamorita, S.; Maxwell, A. C.; Shukla, L.; Morris, J.; Lin, Z.; Marder, T. B.; Steel, P. G. Iridium-catalyzed C–H borylation of quinolines and unsymmetrical 1,2-disubstituted benzenes: insights into steric and electronic effects on selectivity. *Chem. Sci.* **2012,** *3*, 3505–3515. (c) Mkhalid, I. A. I.; Coventry, D. N.; Albesa-Jove, D.; Batsanov, A. S.; Howard, J. A. K.; Perutz, R. N.; Marder, T. B. Ir-Catalyzed Borylation of C-H Bonds in N-Containing Heterocycles: Regioselectivity in the Synthesis of Heteroaryl Boronate Esters. *Angew. Chem. Int. Ed.* **2006,** *45*, 489–491. (d) Harrisson, P.; Morris, J.; Marder, T. B.; Steel, P. G. Microwave-Accelerated Iridium-Catalyzed Borylation of Aromatic C–H Bonds. *Org. Lett.* **2009**, *11*, 3586–3589. (e) Reuven, J. A.; Salih, O. A.; Sadler, S. A.; Thomas, C. L.; Steel, P. G. Exploiting C–H borylation for the multidirectional elaboration of 2-halopyridines. *Tetrahedron* **2020**, *76*, 130836.

(26) Trouvé, J.; Zardi, P.; Al-Shehimy, S.; Roisnel, T.; Gramage-Doria, R. Enzyme-like Supramolecular Iridium Catalysis Enabling C-H Bond Borylation of Pyridines with *meta*-Selectivity. *Angew. Chem. Int. Ed.* **2021**, *60*, 18006–18013.

(27) (a) Shahzadi, H. T.; Fatima, S.; Akhter, N.; Alazmi, M.; Nawaf, A.; Said, K. B.; AlGhadhban, A.; Sulieman, A. M. E.; Saleem, R. S. Z.; Chotana, G. A. Iridium-Catalyzed C–H Borylation of CF3-Substituted Pyridines. *ACS Omega* **2022**, *7*, 11460–11472. (b) Hickey, A.; Merz, J.; Al Mamari, H. H.; Friedrich, A.; Marder, T. B.; McGlacken, G. P. Iridium-Catalyzed Borylation of 6-Fluoroquinolines: Access to 6-Fluoroquinolones. *J. Org. Chem.* **2022**, *87*, 9977–9987. (c) Klecka, M.; Pohl, R.; Klepetarova, B.; Hocek, M. Direct C–H borylation and C–H arylation of pyrrolo[2,3-d]pyrimidines: synthesis of 6,8-disubstituted 7-deazapurines. *Org. Biomol. Chem.* **2009**, *7*, 866–868. (d) Britton, L.; Skrodzki, M.; Nichol, G. S.; Dominey, A. P.; Pawluć, P.; Docherty, J. H.; Thomas, S. P. Manganese-Catalyzed C(sp2)–H Borylation of Furan and Thiophene Derivatives. *ACS Catal.* **2021**, *11*, 6857–6864. (e) Shih, W.-C.; Ozerov, O. V. Selective *ortho* C–H Activation of Pyridines Directed by Lewis Acidic Boron of PBP Pincer Iridium Complexes. *J. Am. Chem. Soc.* **2017**, *139*, 17297–17300. (f) Pang, Y.; Ishiyama, T.; Kubota, L.; Ito,

H. Iridium(I)-Catalyzed C–H Borylation in Air by Using Mechanochemistry. *Chem. Eur. J.* **2019,** *25*, 4654–4659. (g) Murai, M.; Nishinaka, N.; Takai, K. Iridium-Catalyzed Sequential Silylation and Borylation of Heteroarenes Based on Regioselective C–H Bond Activation. *Angew. Chem. Int. Ed.* **2018**, *57*, 5843–5847.

(28) (a) Tamura, H.; Yamazaki, H.; Sato, H.; Sakaki, S. Iridium-Catalyzed Borylation of Benzene with Diboron. Theoretical Elucidation of Catalytic Cycle Including Unusual Iridium(V) Intermediate. *J. Am. Chem. Soc.* **2003**, *125*, 16114–16126. (b) Zhong, R.-L.; Sakaki, S. sp^3 C–H Borylation Catalyzed by Iridium(III) Triboryl Complex: Comprehensive Theoretical Study of Reactivity, Regioselectivity, and Prediction of Excellent Ligand. *J. Am. Chem. Soc.* **2019,** *141*, 9854–9866. (c) Zhu, L.; Qi, X.; Li, Y.; Duan, M.; Zou, L.; Bai, R.; Lan, Y. Ir(III)/Ir(V) or Ir(I)/Ir(III) Catalytic Cycle? Steric-Effect-Controlled Mechanism for the *para*-C–H Borylation of Arenes. *Organometallics* **2017**, *36*, 2107–2115. (d) Wang, G.; Xu, L.; Li, P. Double N,B-Type Bidentate Boryl Ligands Enabling a Highly Active Iridium Catalyst for C–H Borylation. *J. Am. Chem. Soc.* **2015**, *137*, 8058–8061. (e) Green, A. G.; Liu, P.; Merlic, C. A.; Houk, K. N. Distortion/Interaction Analysis Reveals the Origins of Selectivities in Iridium-Catalyzed C–H Borylation of Substituted Arenes and 5-Membered Heterocycles. *J. Am. Chem. Soc.* **2014**, *136*, 4575–4583. (f) Boller, T. M.; Murphy, J. M.; Hapke, M.; Ishiyama, T.; Miyaura, N.; Hartwig, J. F. Mechanism of the Mild Functionalization of Arenes by Diboron Reagents Catalyzed by Iridium Complexes. Intermediacy and Chemistry of Bipyridine-Ligated Iridium Trisboryl Complexes. *J. Am. Chem. Soc.* **2005,** *127*, 14263–14278. (g) Dang, L.; Lin, Z.; Marder, T. B. Boryl ligands and their roles in metal-catalysed borylation reactions. *Chem. Commun.* **2009**, 3987–3995.

(29) (a) Cox, P. A.; Leach, A. G.; Campbell, A. D.; Lloyd-Jones, G. C. Protodeboronation of Heteroaromatic, Vinyl, and Cyclopropyl Boronic Acids: pH-Rate Profiles, Autocatalysis, and Disproportionation. *J. Am. Chem. Soc.* **2016**, *138*, 9145– 9157. (b) Hayes, H. L. D.; Wei, R.; Assante, M.; Geogheghan, K. J.; Jin, N.; Tomasi, S.; Noonan, G.; Leach, A. G.; Lloyd-Jones, G. C. Protodeboronation of (Hetero)Arylboronic Esters: Direct versus Prehydrolytic Pathways and Self-/Auto-Catalysis. *J. Am. Chem. Soc.* **2021**, *143*, 14814–14826. (c) Crabtree, R. H. Deactivation in Homogeneous Transition Metal Catalysis: Causes, Avoidance, and Cure. *Chem. Rev.* **2015,** *115*, 127–150.

(30) Tomasini, M.; Caporaso, L.; Trouvé, J.; Poater, J.; Gramage-Doria, R.; Poater, A. Unravelling Enzymatic Features in a Supramolecular Iridium Catalyst by Computational Calculations. *Chem. Eur. J.* **2022**, *28*, e202201970.

(31) See details in the Supporting Information.

(32) (a) Kadish, K. M.; Shiue, L. R.; Rhodes, R. K.; Bottomley, L. A. Reactions of metalloporphyrin π radicals. 1. Complexation of zinc tetraphenylporphyrin cation and anion radicals with nitrogenous bases. *Inorg. Chem.* **1981**, *20*, 1274–1277. (b) Slagt, V. F.; Reek, J. N. H.; Kamer, P. C. J.; van Leeuwen, P. W. N. M. Assembly of Encapsulated Transition Metal Catalysts. *Angew. Chem. Int. Ed.* **2001**, *40*, 4271–4274. (c) Kadri, M.; Hou, J.; Dorcet, V.; Roisnel, T.; Bechki, L.; Miloudi, A.; Bruneau, C.; Gramage-Doria, R. Palladium-Catalysed Cross-Coupling Reactions Controlled by Noncovalent Zn…N Interactions. *Chem. Eur. J.* **2017**, *23*, 5033–5043. (d) Zardi, P.; Roisnel, T.; Gramage-Doria, R. A Supramolecular Palladium Catalyst Displaying Substrate Selectivity by Remote Control. *Chem. Eur. J.* **2019**, *25*, 627–634.

(33) How the environment affects the chemical shifts of the pyridine **1a** upon binding to zinc remains to be addressed as there is no apparent trend correlating any electronic or steric parameters between the supramolecular ligands **L1**-**L6** with **1a**.

(34) For a unique case of iridium-catalyzed borylation tolerant to water, see: Foley, B. J.; Ozerov, O. V. Air- and Water-Tolerant (PNP)Ir Precatalyst for the Dehydrogenative Borylation of Terminal Alkynes. *Organometallics* **2020**, *39*, 2352–2355.

(35) Ishiyama, T.; Miyaura, N. Iridium-catalyzed borylation of arenes and heteroarenes via C–H activation. *Pure Appl. Chem.* **2006**, *78*, 1369–1375.

(36) (a) Johansson Seechurn, C. C. C.; Sivakumar, V.; Satoskar, D.; Colacot, T. J. Iridium-Catalyzed C–H Borylation of Heterocycles Using an Overlooked 1,10-Phenanthroline Ligand: Reinventing the Catalytic Activity by Understanding the Solvent-Assisted Neutral to Cationic Switch. *Organometallics* **2014**, *33*, 3514–3522. (b) Slack, E. D.; Colacot, T. J. Understanding the Activation of Air-Stable Ir(COD)(Phen)Cl Precatalyst for C–H Borylation of Aromatics and Heteroaromatics. *Org. Lett.* **2021**, *23*, 1561–1565.

(37) (a) Kadish, K. M.; Smith, K. M.; Guillard, R. Handbook of Porphyrin Science, *Vol. 1–44*, World Scientific, Singapore, **2010**–**2016**. (b) Beletskaya, I.; Tyurin, V. S.; Tsivadze, A. Y.; Guillard, R.; Stern, C. Supramolecular Chemistry of Metalloporphyrins. *Chem. Rev.* **2009**, *109*, 1659–1713. (c) Olsson, S.; Dahlstrand, C.; Gogoll, A. Design of oxophilic metalloporphyrins: an experimental and DFT study of methanol binding. *Dalton Trans.* **2018**, *47*, 11572–11585.

(38) For a rare and single case of chlorophilicity in zinc-porphyrins, see: Yamamoto, Y.; Hirata, Y.; Kodama, M.; Yamaguchi, T.; Matsukawa, S.; Akiba, K.-y.; Hashizume, D.; Iwasaki, F.; Muranaka, A.; Uchiyama, M.; Chen, P.; Kadish, K. M.; Kobayashi, N. Synthesis, Reactions, and Electronic Properties of 16 π-Electron Octaisobutyltetraphenylporphyrin. *J. Am. Chem. Soc.* **2010**, *132*, 12627–12638.

(39) (a) Froidevaux, J.; Ochsenbein, P.; Bonin, M.; Schenk, K.; Maltese, P.; Gisselbrecht, J.-P.; Weiss, J. Side Selection of the Fifth Coordinate with a Single Strapped Zinc(II) Porphyrin Host: Full Characterization of Two Imidazole Complexes. *J. Am. Chem. Soc.* **1997**, *119*, 12362–12363. (b) Paul, D.; Melin, F.; Hirtz, C.; Wytko, J.; Ochsenbein, P.; Bonin, M.; Schenk, K.; Maltese, P.; Weiss, J. Induced Fit Process in the Selective Distal Binding of Imidazoles in Zinc(II) Porphyrin Receptors. *Inorg. Chem.* **2003**, *42*, 3779–3787 . (c) Berto, T. C.; Praneeth, V. K. K.; Goodrich, L. E.; Lehnert, N. Iron-Porphyrin NO Complexes with Covalently Attached N-Donor Ligands: Formation of a Stable Six-Coordinate Species in Solution *J. Am. Chem. Soc.* **2009**, *131*, 17116–17126.

(40) (a) Morisue, M.; Morita, T.; Kuroda, Y. Ligand-assisted J-type aggregates of zinc porphyrin: anticooperative molecular organization in self-assembled bolaamphiphile. *Org. Biomol. Chem.* **2010**, *8*, 3457–3463. (b) Summers, J. S.; Stolzenberg, A. M. The *cis*-influence of hydroporphyrin macrocycles on the axial ligation equilibria of cobalt(II) and zinc(II) porphyrin complexes. *J. Am. Chem. Soc.* **1993**, *115*, 10559–10567. (c) Kirksey, C. H.; Hambright, P.; Storm, C. B. Stability constants and proton magnetic resonance studies of zinc *α,β,γ,δ*-tetraphenylporphin and substituted pyridines. *Inorg. Chem.* **1969**, *8*, 2141–2144. (d) Abraham, R. J.; Bedford, G. R.; Wright, B. The NMR spectra of the porphyrins. 17 - Metalloporphyrins as diamagnetic shift reagents, structural and specificity studies. *Org. Magn. Reson.* **1982**, *18*, 45–52. (e) Szintay, G.; Horvath, A. Temperature dependence study of five-coordinate complex formation of zinc(II) octaethyl and tetraphenylporphyrin. *Inorg. Chim. Acta* **2000**, *310*, 175–182.

(41) Yoon, H.; Lee, C.-H.; Jeong, Y.-H.; Gee, H.-C.; Jang, W.-D. A zinc porphyrin-based molecular probe for the determination of contamination in commercial acetonitrile. *Chem. Commun.* **2012**, *48*, 5109–5111. (b) Lee, C.-H.; Lee, S.; Yoon, H.; Jang, W.-D. Strong Binding Affinity of a Zinc–Porphyrin-Based Receptor for Halides through the Cooperative Effects of Quadruple C-H Hydrogen Bonds and Axial Ligation. *Chem. Eur. J.* **2011**, *17*, 13898–13903.

(42) (a) Schmidt, A. F.; Kurokhtina, A. A.; Larina, E. V. Differential selectivity measurements and competitive reaction methods as effective means for mechanistic studies of complex catalytic reactions. *Catal. Sci. Technol.* **2014**, *4*, 3439–3457. (b) 1 mL of toluene as solvent corresponds to 9.4 mmol, as such, in the case of 5 % borylation of toluene, the following formula for the overall selectivity is applied according to Ref. [43a]: $S = (n_{2a+2aa}/n_{pyr})/(n_{borylated\ toluene}/n_{toluene}) = [(0.162\times0.99)/0.162]/[(0.162\times0.05)/9.4] = 1149$. (c) 1 mL of para-xylene as solvent corresponds to 8.11 mmol, as such, in the case of 5 % borylation of toluene, the following formula for the overall selectivity is applied according to Ref. [43a]: S =

$(n_{2a+2aa}/n_{pyr})/(n_{borylated\ para\text{-}xylene}/n_{para\text{-}xylene})$ = [(0.162×0.99)/0.162]/[(0.162×0.05)/8.11] = 991.

(43) Preshlock, S. M.; Ghaffari, B.; Maligres, P. E.; Krska, S. W.; Maleczka Jr., R. J.; Smith III, M. R. High-Throughput Optimization of Ir-Catalyzed C–H Borylation: A Tutorial for Practical Applications. *J. Am. Chem. Soc.* **2013**, *135*, 7572–7582.

(44) The slight difference in these values is due to loss and/or partial protodeboration of the products during purification.

(45) Smith III, M. R.; Maleczka Jr., R. E.; Venkata, A. K.; Onyeozili, E. "Process for Producing Oxazole, Imidazole, Pyrazole Boryl Compounds". US Pat. 7,709,654B2, **2008**.

(46) (a) Mayr, H.; Ofial, A. R. The Reactivity–Selectivity Principle: An Imperishable Myth in Organic Chemistry. *Angew. Chem. Int. Ed.* **2006**, *45*, 1844–1854. (b) Mayr, H.; Breugst, M.; Ofial, A. R. Farewell to the HSAB Treatment of Ambident Reactivity. *Angew. Chem. Int. Ed.* **2011**, *50*, 6470–6505.

(47) (a) Abuhafez, N.; Perennes, A.; Gramage-Doria, R. Mimicking Enzymes: Taking Advantage of the Substrate-Recognition Properties of Metalloporphyrins in Supramolecular Catalysis. *Synthesis* **2022**, *54*, 3473–3481. (b) Longevial, J.-F.; Clément, S.; Wytko, J. A.; Ruppert, R.; Weiss, J.; Richeter, S. Peripherally Metalated Porphyrins with Applications in Catalysis, Molecular Electronics and Biomedicine. *Chem. Eur. J.* **2018**, *24*, 15442–15460.

(48) (a) Dydio, P.; Reek, J. N. H. Supramolecular control of selectivity in transition-metal catalysis through substrate preorganization. *Chem. Sci.* **2014**, *5*, 2135–2145. (b) Davis, H. J.; Phipps, R. J. Harnessing non-covalent interactions to exert control over regioselectivity and site-selectivity in catalytic reactions. *Chem. Sci.* **2017**, *8*, 864–877. (c)Trouvé, J.; Gramage-Doria, R. Beyond hydrogen bonding: recent trends of outer sphere interactions in transition metal catalysis. *Chem. Soc. Rev.* **2021**, *50*, 3565–3584. (d) Olivo, G.; Capocasa, G.; Del Giudice, D.; Lanzalunga, O.; Di Stefano, S. New horizons for catalysis disclosed by supramolecular chemistry. *Chem. Soc. Rev.* **2021**, *50*, 7681–7724. (e) Jiao, Y.; Chen, X.-Y.; Stoddart, J. F. Weak bonding strategies for achieving regio- and site-selective transformations. *Chem* **2022**, *8*, 414-438. (f) van Leeuwen, P. W. N. M.; Raynal, M. *Supramolecular Catalysis: New Directions and Developments*, Wiley-VCH, Weinheim, **2022**.

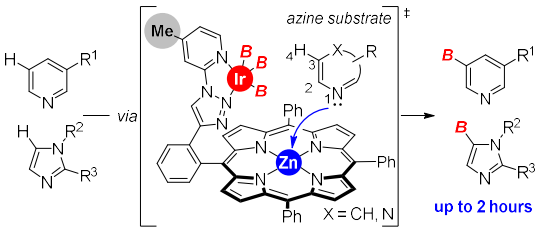

$[Ir(COD)(Cl)]_2$ outperforms $[Ir(COD)(OMe)]_2$ w/o incubation time: kinetics, additives
Multiple deactivation pathways identified (NMR, X-ray) and circumvented
Atom-precise selectivity analyzed by DFT: NCI beyond the molecular recognition site
Selectivity imposed by molecular recongition site at the 2nd coordination sphere
Activity imposed by 4-Me substitution instead of the classic 4-tBu pattern